



1 **Extending planktic foraminiferal Mg/Ca palaeothermometry into polar**
2 **temperature ranges: crust- and lamellae specific calibrations and non-**
3 **thermal controls**

4

5 Adele Westgård^{1*}, Mohamed M. Ezat¹, Freya E. Sykes¹, Julie Meilland^{2,3}, Thomas B. Chalk^{1,3}, J. Andy
6 Milton⁴, Melissa Chierici⁵, Gavin L. Foster⁴

7 *Correspondence to: adele.westgard@uit.no

8 ¹ iC3: Centre for ice, Cryosphere, Carbon and Climate, Department of Geosciences, UiT The Arctic University of
9 Norway, 9037 Tromsø, Norway

10 ² MARUM – Center for marine environmental sciences, University of Bremen, Leoberner str. 8 Bremen 28359,
11 Germany

12 ³ Aix Marseille Université, CNRS, IRD, INRAE, CEREGE, Technopole Environnement Arbois-Méditerranée BP
13 80 13545 Aix-en-Provence, Cedex 04, France

14 ⁴ School of Ocean and Earth Science, National Oceanography Centre Southampton, University of Southampton,
15 Southampton SO 3ZH, England

16 ⁵ Institute of Marine Research, Oceanography and Climate Research Group, Fram Centre, Hjalmar Johansens gate
17 14, 9007, Tromsø, Norway

18

19



20 Abstract

21 The rapidity of climate change in the polar regions underscores the need for improved understanding of
22 its impacts on ocean circulation at both regional and global scales. Reconstructions of past polar ocean-
23 cryosphere interactions can provide this context, but large uncertainties in existing proxies limit the
24 utility of such studies. For instance, there are currently no low-temperature ($<9^{\circ}\text{C}$) culture-based Mg/Ca-
25 calibrations for planktic foraminifera, a key tool for reconstructing past changes in ocean temperatures.
26 There is also limited understanding of non-thermal influences on Mg/Ca in *Neogloboquadrina*
27 *pachyderma*, the only modern polar planktic foraminifera. Moreover, this species exhibits considerable
28 levels of heterogeneity in composition precipitating a thick lower-Mg/Ca outer crust over higher Mg/Ca
29 inner lamellae calcite; specimens with predominantly, albeit variable crust–lamellae proportions, are
30 thus thought to introduce substantial uncertainty into high-latitude palaeotemperature reconstructions.
31 Here, we used *N. pachyderma* cultured across a range of temperatures, salinities, and carbonate
32 chemistry conditions including experiments in which pH and $[\text{CO}_3^{2-}]$ either covaried or were decoupled.
33 By using a laser ablation approach to analyse crust and lamellae separately, we present new Mg/Ca-
34 temperature calibrations for each component that extend culture-based calibrations in *N. pachyderma*
35 down to the lower temperature-range ($2\text{--}9^{\circ}\text{C}$). The crust-specific calibration is of particular importance
36 in high-latitude downcore records where *N. pachyderma* are commonly observed to preserve
37 predominantly or only crust. Our results show significant carbonate chemistry influence on Mg/Ca with
38 opposite influences from pH and carbonate ion concentration, when these variables changed in isolation.
39 Additionally, we show that environmental conditions regulate crust-lamellar proportions, where
40 increased salinity and temperature, and lower pH lead to less crust formation with implications for future
41 ocean acidification and Arctic Atlantification, and for downcore reconstructions.

42

43



44 1 Introduction

45 Understanding of polar surface ocean hydrography, and ocean-cryosphere interactions are crucial to
46 assessing the implications of ongoing high-latitude warming. Studying past climate change in the polar
47 regions provides invaluable insights into these processes (e.g., Ezat et al., 2024; Stein, 2019; Hou et al.,
48 2025). However, there are several challenges to studying polar palaeoceanography, including limited
49 access due to the remoteness and prolonged sea ice cover, low sedimentation rates of deep ocean
50 sediments, and preservation biases of common proxy carriers such as the dissolution of calcareous
51 fossils (e.g., Stein, 2019). This is particularly true for the magnesium to calcium ratio (Mg/Ca) of
52 foraminifera shells, a key proxy used to reconstruct paleotemperature (e.g., Elderfield and Ganssen,
53 2000), that results in a range of unrealistic values in the polar regions when applying existing calibrations
54 (e.g., Prabhakar et al., 2024).

55 The polar planktic foraminifera *Neogloboquadrina pachyderma* is the most abundant species of planktic
56 foraminifera in the high latitude oceans and often the only planktic species available in polar
57 sedimentary records (e.g., Chaabane et al., 2024; Kucera, 2007). It is therefore a key species for
58 reconstructing past surface hydrography in the high latitudes (Eynaud et al., 2009; Kohfeld et al., 1996;
59 Rodríguez-Sanz et al., 2012). Its habitat extends from equatorial upwelling zones to polar waters, and
60 dominates the planktic foraminifera assemblage at temperatures $<5^{\circ}\text{C}$ (Greco et al., 2019; Kucera et al.,
61 2005; Anglada-Ortiz et al., 2023). Studies have also suggested that *N. pachyderma* adjusts its depth
62 habitat in response to food-availability and productivity, sea-ice, and sea surface temperature (SST)
63 hence reducing its representation of actual SSTs (Greco et al., 2019; Anglada-Ortiz et al., 2023). *N.*
64 *pachyderma* is a resilient and opportunistic species which has been found to: live in sea ice, in marine
65 snow/aggregate microhabitats, and utilise behaviours such as dormancy, ectoplasmic structures, and
66 asexual reproduction to survive unfavourable conditions and/or quickly recover its population (e.g.,
67 Greco et al., 2023; Meilland et al., 2022; Westgård et al., 2023; Davis et al., 2020; Spindler and
68 Dieckmann, 1986). These strategies may impact the environmental signals recorded by its shell
69 geochemistry through, for example, extended life cycle due to dormancy and extreme habitat conditions



70 (e.g., high salinity, high pH) in the sea ice (Spindler and Dieckmann, 1986; Bertlich et al., 2021;
71 Westgård et al., 2023).

72 The combination of biological processes and life cycle behaviours of foraminifera cause a range of non-
73 environmental variability in shell geochemical composition often referred to as the collective term “vital
74 effects” (e.g., Kozdon et al., 2009b; Branson et al., 2025). In *N. pachyderma* this arises from, for
75 example, the thick crust it forms towards the end of its life cycle covering the outer portions of its shell
76 with a markedly different geochemical composition from the initial lamellar calcite (Hupp and
77 Fehrenbacher, 2023, 2024; Jonkers et al., 2016; Kozdon et al., 2009a; Kozdon et al., 2009b; Westgård
78 et al., 2026). For instance, it is commonly observed that the Mg/Ca ratio of the crust is substantially
79 lower than the lamellar calcite (Hupp and Fehrenbacher, 2023, 2024; Jonkers et al., 2016; Kozdon et al.,
80 2009a; Livsey et al., 2020; Davis et al., 2017; Westgård et al., 2026).

81 Westgård et al. (2026) showed that when the crust and lamellar calcite grew in the same environmental
82 conditions, the observed geochemical difference persisted, implying the observed compositional
83 variations resulted from contrasting biomineralisation processes rather than environmental influences
84 from, for example, vertical migration in the water column. For any given Mg/Ca calibration, the lower
85 Mg/Ca crust yields lower temperatures than the higher Mg/Ca lamellar calcite from the same specimen
86 and population, even when grown at equivalent conditions. The laboratory-based study also found that
87 the difference between the two components decreases with increasing temperature and is insignificant
88 at the higher temperatures inhabited by the species (Westgård et al., 2026). As Mg/Ca increases
89 exponentially with temperature, Mg/Ca-temperature calibrations are less sensitive at the lower
90 temperature-range. The larger difference between crust and lamellar calcite Mg/Ca at lower
91 temperatures therefore lead to additional uncertainties in temperature estimates based on both
92 components.

93 The geochemistry of the test is often dominated by the crust, that accounts for ~40–80% of the total
94 shell mass (e.g., Kozdon et al., 2009a; Hupp and Fehrenbacher, 2023) and can vary within and between
95 samples downcore (Westgård et al., 2026). The varying ratio between the two components makes it
96 challenging to account for the geochemical difference between the crust and lamellar calcite, for



97 example by assuming a constant volume fraction. The difference in geochemical composition between
98 the two components, and the proportion of crust are therefore underappreciated sources of inaccuracy
99 and uncertainty in *N. pachyderma* and must be considered in application and development of
100 geochemical proxy calibrations.

101 Westgård et al. (2026) proposed a method to separate the two components in element/Ca profiles
102 obtained from Laser Ablation Inductively Coupled Plasma Mass Spectrometry (LA ICP-MS) which
103 opened the possibility of developing and applying proxy-calibrations for the two components
104 independently. This is in line with previous studies, which suggests that using the components separately
105 can reduce uncertainty and inaccuracy in temperature estimates (e.g., Livsey et al., 2020; Jonkers et al.,
106 2016).

107 Most existing calibrations of the Mg/Ca temperature relationship (Table 1) are based on whole-shell
108 measurements of *N. pachyderma* (and other species) from core top or sediment trap samples (e.g., Anand
109 et al., 2003; Elderfield and Ganssen, 2000; Kozdon et al., 2009a; Vázquez Riveiros et al., 2016; Lea et
110 al., 1999; Jonkers et al., 2013) or a combination of tow, sediment trap, core top, and/or culture samples
111 (Morley et al., 2024; Tierney et al., 2019). Although, there are two Mg/Ca calibrations based on the
112 lamellar calcite only from plankton tow and laboratory-grown specimens (c.f., Livsey et al., 2020; Davis
113 et al., 2017). There are however currently no culture-based Mg/Ca calibrations below 9°C (see Table 1)
114 for *N. pachyderma* and no calibrations that consider the crust only, or both components calcite
115 independently. This is desirable because the crust component is the largest, by mass, and the lamella
116 component is preferentially lost during sample cleaning and early diagenesis (c.f., Fritz-Endres and
117 Fehrenbacher, 2021).

118 Other environmental factors have also been shown to influence the Mg/Ca ratio in foraminifera, e.g.,
119 salinity (Hönisch et al., 2013; Peral et al., 2022; Allen et al., 2016) and seawater carbonate chemistry
120 (e.g., Allen et al., 2016; Holland et al., 2020; Morley et al., 2024; Russell et al., 2004; Evans et al., 2016;
121 Haynes et al., 2023). Some authors have developed calibrations which consider corrections for such
122 non-thermal influences on Mg/Ca in *N. pachyderma* and other species (e.g., Morley et al., 2024; Tierney
123 et al., 2019; Davis et al., 2017).



124 Because only a few culture studies exist for *N. pachyderma*, and to our knowledge only one study,
125 Westgård et al. (2026), document geochemical signals in laboratory-grown crust, the influence of the
126 aforementioned thermal and non-thermal influences on Mg/Ca in both the crust and lamellar calcite
127 remain poorly constrained.

128 Here we present Mg/Ca-environmental relationships from extensive culture experiments (Table S1 and
129 2) conducted in 2021 and 2022 across a range of temperatures (2–9°C), carbonate chemistry ($[\text{CO}_3^{2-}]$
130 64–243 $\mu\text{mol/kg}$; pH 7.65–8.4), and salinities (29.8–36.7) encompassing realistic past and future
131 conditions of the polar environments (e.g., Amap, 2018; Stein, 2019). The results presented in this study
132 are produced using the data processing method presented in Westgård et al. (2026, Table S1). Mg/Ca
133 data from all salinities, carbonate chemistries, and temperatures 2 and 7°C, and all Mg/Ca-
134 environmental parameter relationships are presented for the first time in this study (Table S1). Mean
135 Mg/Ca from temperature treatments 4.5, 6, and 9°C were first presented in Westgård et al. (2026) in
136 relation to method development and studying the differences between crust and lamellae calcification
137 (Table S1) and are available through the open data repository DataverseNO at:
138 <https://doi.org/10.18710/IYDI4O>. Biological observations from 2021 experiments are presented in
139 Westgård et al. (2023, Table S1).

140 By using a laser ablation approach, we provide new *N. pachyderma* Mg/Ca-temperature calibrations for
141 polar conditions with separate calibrations for the crust and lamellar calcite (Table S1). In addition to
142 thermal influences, we quantify the effects of salinity and carbonate chemistry on Mg/Ca.



143 Table 1. A selection of existing Mg/Ca-based temperature calibrations. T = temperature, S = salinity, N = sample size, Ω_{Ca} = calcite saturation state, $[CO_3^{2-}] =$
 144 carbonate ion concentration, *N. p.* = *Neogloboquadrina pachyderma*, *N. i.* = *Neogloboquadrina incompta*. See also Fig. 4.

Study	Equation Mg/Ca (mmol/mol) =	T range (°C)	Culture/ coretop/ sediment trap	Other environmental factors (S, pH, [CO ₃ ²⁻])	Species	N	Solution/ laser	Crust/ lamellar/ both	Notes
(Livsey et al., 2020)	$1.93 * \exp^{(0.082T)}$	-1.81 to 3.80	low		<i>N. p.</i>	41	laser	lamellar	
(Kozdon et al., 2009a)	$0.13T + 0.35$	>3, 3-6	Core top	$\delta^{44}Ca$ for depth	<i>N. p.</i>	20 with 60-80 specimens	solution	both	
(Jonkers et al., 2013)	$0.60 * \exp^{(0.09T)}$	5-10	Sediment trap		<i>N. p.</i>	20 samples of 20-40 specimens	solution	both	
(Tierney et al., 2019)	BAYMAG code on github	-0.9 to 15.3	Culture + coretop	S, pH, bottom water Ω_{Ca}	Multi and <i>N. p.</i> + <i>N. i.</i>	119 + 12	both	both	Bayesian model
(Morley et al., 2024)	$Mg/Ca^{(CO_3^{2-})} = 3227.95 * [CO_3^{2-}]^{1.53} - 0.327 * \exp^{(0.0936T)}$	-2 to 16	Tow + core top	[CO ₃ ²⁻]	<i>N. p.</i> + <i>N. i.</i>	235	solution	Both, correction -1.5%	Requires [CO ₃ ²⁻] proxy ($\delta^{18}O$)
(Davis et al., 2017)	$0.71 * T - 2.49$	(6) 9 - 12	culture		<i>N. p.</i>	10	laser	lamellar	No chamber addition was reported at 6°C, thus there is large uncertainty in the calibration below 9°C.

145



146 2 Methods

147 Sample collection and experiments were conducted during summers 2021 and 2022 and specimens were
148 sampled from 74.5°N, 01.6°E (Ezat et al., 2021) and 72.5°N, 00.0°E (Ezat et al., 2022) aboard the RV
149 Helmer Hanssen. The protocol of sample collection and culture methods for 2021 experiments are
150 presented in Westgård et al. (2023) and culture protocol for temperatures 6 and 9°C (2022) experiments
151 and trace element analysis are presented in Westgård et al. (2026). See overview in Table S1. All
152 experimental procedures were similar and are described herein for completeness.

153

154 2.1 Foraminifera sampling and culturing

155 Small (<120 µm), healthy specimens (i.e., with bright orange cytoplasm and extensive rhizopodial
156 network) of *Neogloboquadrina pachyderma* were collected using a WP2 plankton net (64µm mesh) and
157 placed into individual 70 mL culture bottles pre-filled with culture media (chemistry controlled filtered
158 sea water). Upon return to the laboratory at UiT The Arctic University of Norway, specimens were
159 placed into light and temperature-controlled Friocell EVO incubators set at 2–9°C (see detailed culture
160 conditions in Table 2). Water treatments were prepared with independently variable parameters intended
161 to reflect realistic past and future conditions with salinities of 29.8–36.7, pH of 7.65–8.4 (total scale),
162 [CO₃²⁻] of 64–243 µmol/kg, where we also altered pH and [CO₃²⁻] independently of each other.

163 To ensure calcification only occurred in intended conditions, water was replaced every 2–6 days and.
164 experiments were terminated in case of any pH drift >0.05 from the intended value. Dead specimens
165 (i.e. shells appearing empty) were rinsed in distilled water and placed individually in
166 micropalaeontological slides.

167

168 2.2 Preparation and monitoring of culture media:

169 Seawater for culture media was immediately filtered (2 µm cellulose filters) and stored in opaque 20L
170 cans at 4°C. Water samples were collected for elemental composition (Table 3) and carbonate chemistry



171 (Table 2, Fig. S1) prior to, during, and at the end of the experiments. Each set of experiments had a
172 dedicated “ambient” treatment (pH ~8.1, salinity ~35 and temperature 4.5°C in 2021 and 6°C in 2022),
173 with conditions closely matching those at the foraminiferal collection site. Salinity and carbonate
174 chemistry experiments were performed at two different temperatures, i.e., 4.5°C (2021) and 6°C (2022).
175 Incubator temperatures were set to 2, 4.5, 6, 7, and 9°C (Table 2) and remained stable throughout the
176 experiments. Instrumentation error is <0.5°C spatially and <0.2°C temporally. The LED light
177 programme was set to mimic the high-latitude summer conditions.

178 Salinity of the culture media (Table 2) was increased by adding brine from partial freezing of filtered
179 seawater and lowered by the additional of the melt of the ice fraction with the aim to replicate conditions
180 produced during sea ice formation as closely as possible. For the salinity experiments performed in
181 2021, salinity was also decreased by addition of distilled water and increased by addition of brine
182 produced from evaporation of seawater on a hotplate (c.f., Westgård et al., 2023). This resulted in seven
183 treatments with variable salinity: 29.8, 32.5, 33.6, 36.7 (from the partial freezing of seawater approach),
184 30.4 and 32.1 (addition of distilled water), 36.7 (brine from evaporated seawater), plus the two ambient
185 treatments at 35.0 (4°C), and 35.4 (6°C).

186 Carbonate chemistry of the culture media (Table 2) was modified in three ways with the intended
187 outcomes of: 1) altering pH and other carbonate parameters by addition of HCl to decrease pH or NaOH
188 to increase pH, resulting in concurrent changes in pH and carbonate ion concentration ($[\text{CO}_3^{2-}]$); 2)
189 altering pH while forcing $[\text{CO}_3^{2-}]$ to remain constant by addition of HCl or NaOH and adjusting $[\text{CO}_3^{2-}]$
190] by addition of artificial seawater (a mixture of distilled water and salt) or NaHCO_3 ; or 3) altering $[\text{CO}_3^{2-}]$
191] while keeping pH stable, by addition of NaHCO_3 or artificial seawater.

192 This resulted in five treatments where pH and $[\text{CO}_3^{2-}]$ co-varied (pH 7.78, 7.83, 7.84, 8.04, 8.10, 8.26,
193 and 8.40), three treatments of variable $[\text{CO}_3^{2-}]$ at stable pH (64, 195, 206 $\mu\text{mol/kg}$ at pH 8.07 ± 0.13) and
194 three treatments with variable pH at relatively stable $[\text{CO}_3^{2-}]$ (pH 7.65, 7.88, 8.15 at $[\text{CO}_3^{2-}] = 129 \pm 22$
195 $\mu\text{mol/kg}$).

196 *Isotope labelling*



197 All experimental water were labelled with ^{135}Ba -isotope spike where $^{135}\text{Ba}_{\text{sw},95} = \%$ of total Ba, in order
198 to distinguish laboratory-grown calcite from ocean-grown calcite, resulting in $^{135}\text{Ba}_{\text{sw}}$ of 1.16 μmol and
199 1.97 μmol in 2021 and 2022 respectively (c.f., Westgård et al., 2026).

200

201 2.3 Analysis of water samples:

202 Water samples taken for carbonate chemistry (Table 2, Fig. S1) and elemental composition (Table 3)
203 were analysed at the Institute of Marine Research (IMR) in Tromsø, Norway and the Centre for Earth
204 Research and Analysis (CERAS) at the University of Southampton, UK, respectively, for detailed
205 procedures refer to Westgård et al. (2026).

206 Samples for determining carbonate chemistry were analysed for total alkalinity (TA) and dissolved
207 inorganic carbon (DIC) following protocols described in Dickson et al. (2007). All other carbonate
208 system parameters were calculated in CO2SYS software (CO2SYS program, Pierrot et al., 2006) with
209 paired TA and DIC, salinity, and experimental temperature. Due to extreme high DIC in the pH 7.6
210 treatment with decoupled $[\text{CO}_3^{2-}]$, total alkalinity (TA) was not measured. This variable and the
211 remaining carbonate system parameters calculated from DIC measured at IMR were combined with pH
212 on total scale measured during experiments using a handheld Metrohm 914 pH-meter at experimental
213 temperature (6°C).

214 Water samples for element analysis were analysed using an Agilent 8900 Triple Quadrupole (QQQ) ICP-
215 MS in He-gas mode to achieve acceptable sensitivity for Mg/Ca (Table S2). Based on analysis of the
216 SOTON-SW internal sea water standard, the long-term accuracy for Mg, Ca, and Ba is $<7\%$.
217 Reproducibility is $<10\%$ (2SD) for Mg and Ca (at ≥ 0.2 ppm).

218



219 *Table 2. Water conditions including temperature, salinity, and carbonate chemistry, for all water treatments. The method used to modify salinity treatments is*
 220 *indicated in the "comments" column. *Ambient treatments for years 2021 and 2022, with conditions closely matching those at the foraminiferal collection site.*
 221 ***TA, HCO₃⁻, and Ω_{calcite} are estimated values based on measured DIC, pH measured during experiments, and experimental temperature (see section 2.3); DIC,*
 222 *TA and pH were measured for all other treatments. See treatment correlations and scatter matrix of water treatments in Fig. S1. pH_T = pH on total scale, TA =*
 223 *total alkalinity, DIC = dissolved inorganic carbon, [CO₃²⁻] = carbonate ion concentration, [HCO₃⁻] = bicarbonate ion concentration, Ω_{calcite} = calcite saturation*
 224 *state, T = temperature.*

Variable	Year	Salinity	DIC (μmol/kg)	TA (μmol/kg)	pH _T	[CO ₃ ²⁻] (μmol/kg)	[HCO ₃ ⁻] (μmol/kg)	Ω _{calcite}	T (°C) ±0.5	Comments
Temperature	2021	35.0 ±0.7	2213 ±40	2391 ±20	8.16 ±0.05	130 ±12	2065 ±52	3.1 ±0.3	2	Distilled water
	*2021	35.0 ±0.7	2213 ±40	2391 ±20	8.10 ±0.05	130 ±12	2065 ±52	3.1 ±0.3	4.5	
	*2022	35.4 ±0.1	2158 ±12	2338 ±22	8.04 ±0.07	138 ±17	1997 ±35	3.3 ±0.4	6	
salinity	2021	35.0 ±0.7	2213 ±40	2391 ±20	8.08 ±0.05	130 ±12	2065 ±52	3.1 ±0.3	7	Melted «sea-ice»
	2021	35.4 ±0.1	2158 ±12	2338 ±22	8.09 ±0.07	138 ±17	1997 ±35	3.3 ±0.4	9	
	2021	29.8 ±0.1	1902 ±28	2043 ±5	8.12 ±0.07	102 ±13	1784 ±39	2.5 ±0.3	4.5	
pH and carbonate ion concentration	2021	30.4 ±0.1	1952 ±17	2051 ±1	7.96 ±0.05	86 ±9	1837 ±22	2.2 ±0.2	6	Melted «sea-ice»
	2021	32.1 ±0.1	2038 ±27	2197 ±8	8.12 ±0.05	115 ±11	1906 ±35	2.8 ±0.3	4.5	
	2022	32.5 ±0.0	2127 ±21	2273 ±6	8.03 ±0.07	117 ±16	1985 ±34	2.8 ±0.3	6	
pH (decoupled carbonate ion concentration)	2021	33.6 ±0.0	2136 ±20	2332 ±4	8.17 ±0.04	140 ±10	1980 ±28	3.4 ±0.2	4.5	Melted «sea-ice»
	2021	36.7 ±0.1	2330 ±16	2494 ±0	8.04 ±0.04	124 ±9	2184 ±23	2.9 ±0.2	4.5	
	2021	36.7 ±0.5	2267 ±21	2439 ±25	8.07 ±0.01	127 ±3	2120 ±18	3.0 ±0.1	4.5	
Carbonate ion concentration	2022	35.4 ±0.1	2177 ±35	2241 ±24	7.78 ±0.04	73 ±6	2059 ±35	1.8 ±0.1	6	Evaporated brine
	2022	35.3 ±0.1	2183 ±8	2264 ±2	7.83 ±0.03	82 ±5	2061 ±10	2.0 ±0.1	6	
	2021	35.0 ±0.1	2193 ±35	2270 ±21	7.84 ±0.04	72 ±17	2087 ±48	1.7 ±0.4	4.5	
pH (decoupled carbonate ion concentration)	2022	35.4 ±0.1	2300 ±40	2583 ±3	8.26 ±0.07	211 ±24	2073 ±62	5.1 ±0.6	6	Evaporated brine
	2021	35.0 ±0.1	2218 ±8	2567 ±5	8.40 ±0.01	243 ±2	1966 ±9	5.8 ±0.0	4.5	
	2022	36.7 ±0.1	1641 ±22	1716 ±3	7.83 ±0.08	64 ±11	1547 ±27	1.5 ±0.3	6	
pH (decoupled carbonate ion concentration)	2022	35.4 ±0.2	2890 ±11	3124 ±5	8.12 ±0.02	195 ±8	2668 ±17	4.7 ±0.2	6	Evaporated brine
	2022	35.2 ±0.2	3406 ±14	3635 ±1	8.07 ±0.02	206 ±9	3163 ±21	4.9 ±0.2	6	
	**2022	35.4 ±0.1	4772 ±10	4800	7.65	129	4514	3.1	6	
pH (decoupled carbonate ion concentration)	2022	35.2 ±0.2	3558 ±10	3688 ±1	7.88 ±0.02	147 ±6	3352 ±13	3.5 ±0.1	6	Evaporated brine
	2022	36.8 ±0.4	1229 ±19	1388 ±2	8.15 ±0.05	93 ±8	1126 ±26	2.2 ±0.2	6	



226 2.4 Foraminiferal sample preparation and Laser Ablation ICP-MS analyses

227 Foraminiferal specimens were individually cleaned using 400 µl oxidative reagent (1:1 30% H₂O₂ and
228 0.1M NaOH) in a water bath (65°C) for four 2.5-minute intervals (c.f., Westgård et al., 2026; Barker et
229 al., 2003). The reagent was then removed, and specimens rinsed 3 times in ~1mL 18.2 MΩcm MilliQ-
230 water. Specimens were mounted on glass slides using double-sided cellulose tape prior to laser ablation.
231 The final 2–4 chambers of the shell whorl were analysed using a spot size of 30 µm at 10% intensity
232 with an energy density of 0.8 mJ/cm² and a repetition rate of 5 Hz. The dwell time for analysis was 40
233 seconds for thinner, non-crust shells and 60 seconds for thicker, crusted shells (c.f., Westgård et al.,
234 2026). Every ~100 ablations were bracketed by analysis of reference materials NIST SRM 610, NIST
235 SRM 612 (measured at 20% intensity), pressed carbonate powder pellets of JCP-1 (*porites sp.*, GSJ,
236 Okai et al., 2002) and JCT-1 (*Tridacna gigas*, GSJ, Inoue et al., 2004), and USGS MACS-3 carbonate
237 pellet (Jochum et al., 2005). Ablations were followed by a 30-second wash out. This study is based on
238 ²⁴Mg, ⁴³Ca, ¹³⁵Ba, and ¹³⁸Ba.

239

240 2.5 Data processing and analysis

241 Exported time resolved data in counts per second were processed using iolite 4 (Paton et al., 2011; Paul
242 et al., 2023). Raw element data were normalised to ⁴⁴Ca and then calibrated using NIST610, NIST612
243 and JCP-1. JCT-1 and MACS-3 were analysed as unknowns for quality control. Mg/Ca is within <10%
244 of reference values for JCT-1 (2022), and within <20% for MACS-3 (2021, and 2022, c.f., Westgård et
245 al., 2026).

246 Further data processing and analysis were performed in R (Rcoreteam, 2022). Laboratory-grown calcite
247 was identified, and crust and lamellar calcite were distinguished using open source code LabGrown and
248 IDCrust developed by Westgård et al. (2026) (<https://github.com/Adele-W/Westgard-et-al.-2025>). In
249 this study, data is presented for the laboratory-grown shells in three categories: crust (CC), lamellar
250 calcite (LC), and both components combined (CC + LC). Not all laboratory-grown chambers were
251 encrusted, and in some chambers, there was laboratory-grown crust on top of ocean-grown lamellar



252 calcite. The category for both components (CC + LC) therefore only include shells where both
253 components were present and grown under laboratory conditions. Shell thickness was estimated based
254 on length of the shell profile and ablation rate (0.4 $\mu\text{m}/\text{sec}$, c.f., Westgård et al., 2026). The crust
255 thickness (proportion as % of total shell thickness) was estimated using the length of the shell profile
256 and the crust-lamellar boundary (breakpoint) identified by IDCrust.

257 Distribution coefficients D_{Mg} were calculated for each water treatment (Table 3) according to equation
258 1, e.g., Branson et al. (2025).

$$259 \quad D_{\text{element}} = \frac{\text{element}/\text{Ca}_{\text{calcite}}}{\text{element}/\text{Ca}_{\text{seawater}}} \quad (1)$$

260 Scatterplots exploring co-variance of water treatments, environmental conditions and Mg/Ca, as well as
261 regression lines for Mg/Ca relationships with environmental conditions were plotted and modelled using
262 R. The best fit model produced in R also provides statistical test parameters for Pearsons R, standard
263 error, t-test, and p-values where relevant. Pseudo- R^2 for non-linear relationships were calculated using
264 the residual sum of squares divided by the total sum of squares. The environmental relationships are
265 presented in three ways: 1) Mg/Ca ratios for all ablated chambers; 2) the median Mg/Ca in each water
266 treatment; and 3) the distribution coefficients.

267

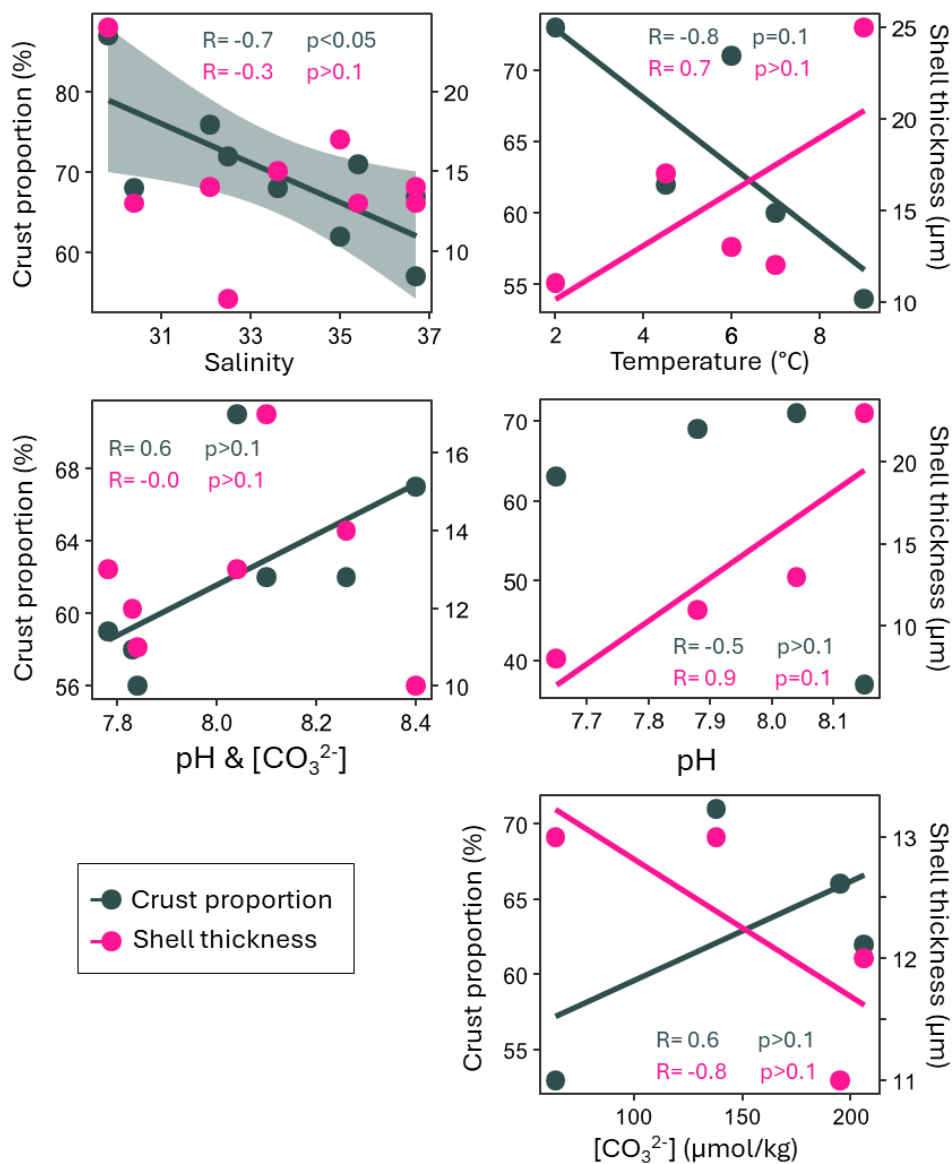
268 3 Results

269 3.1 Environmental influence on crust formation

270 The total number of laboratory-grown chambers was 525 and the number of crusted chambers is 279
271 (Table S3). We observe crust growth in all treatments; the pH 8.15 treatment without co-varying
272 carbonate ion had the lowest number of crusted chambers (21% of measured chambers, Table 3 & S3),
273 while all chambers were crusted in the high salinity (36.7) treatment from evaporated seawater and the
274 salinity 33.6 treatment. From the 525 analysed laboratory-grown chambers, in 154 chambers only crust
275 was identified from the LabGrown & IDCrust algorithms, suggesting these chambers were characterized
276 by laboratory grown crust that was added onto ocean grown lamellae, that the chamber wall was not



277 ablated through, or alternatively they consisted of predominantly crust. Based on tests were both crust
278 and lamellar calcite was analysed (and laboratory-grown), we observe that the total shell thickness
279 **decreases** with decreasing pH and temperature ($|R| > 0.5$, $p > 0.05$). We also observe decreased total shell
280 thickness with increasing $[\text{CO}_3^{2-}]$ ($R = -0.8$, $p > 0.05$). There is no statistically significant change in total
281 shell thickness with changing salinity. We observe significantly lower proportions of crust in the shell
282 at higher salinities compared to low salinities ($R = -0.7$, $p < 0.05$). We also observe a decrease in the
283 proportion of crust with decreasing pH and/or $[\text{CO}_3^{2-}]$, and higher temperatures ($|R| > 0.5$, $p > 0.05$, Fig.
284 1).



285

286 *Figure 1. Mean crust proportion (as % of total shell thickness) and total shell thickness (µm) in each*
 287 *water treatment correlated with environmental conditions. The plot includes only specimens where both*
 288 *the crust and lamellae were laboratory-grown. Trend lines are included for relationships where |R| > 0.5.*
 289 *Significant relationships have a 95% confidence envelope in green shading. See corresponding data in*
 290 *table 3 & S3.*

291



292 **3.2 Culture media and Distribution coefficients**

293 The conditions and elemental composition of culture media is presented in Tables 2 and S1. Some
294 salinity and pH with co-varying $[\text{CO}_3^{2-}]$ experiments were therefore carried out at different temperatures
295 (4.5 or 6°C). We observe minimal difference in seawater Mg/Ca between the two experimental years
296 (5084±549 and 5024±107 mmol/mol in 2021 and 2022 respectively; Table S2) and higher seawater
297 Mg/Ca in culture media compared to natural seawater (4788±102 mmol/mol) from the 2021 collection
298 site.

299



300 *Table 3. Median Mg/Ca (mmol/mol), Distribution coefficients (D_{Mg}) for element ratios in seawater*
 301 *treatments to foraminiferal calcite, and shell structure per water treatment. For each Mg/Ca and D_{Mg}*
 302 *crust (CC), lamellar calcite (LC), and both components combined (CC+LC) are listed separately. 36-f*
 303 *and 36-e were prepared using rejection brine and evaporated seawater respectively.*

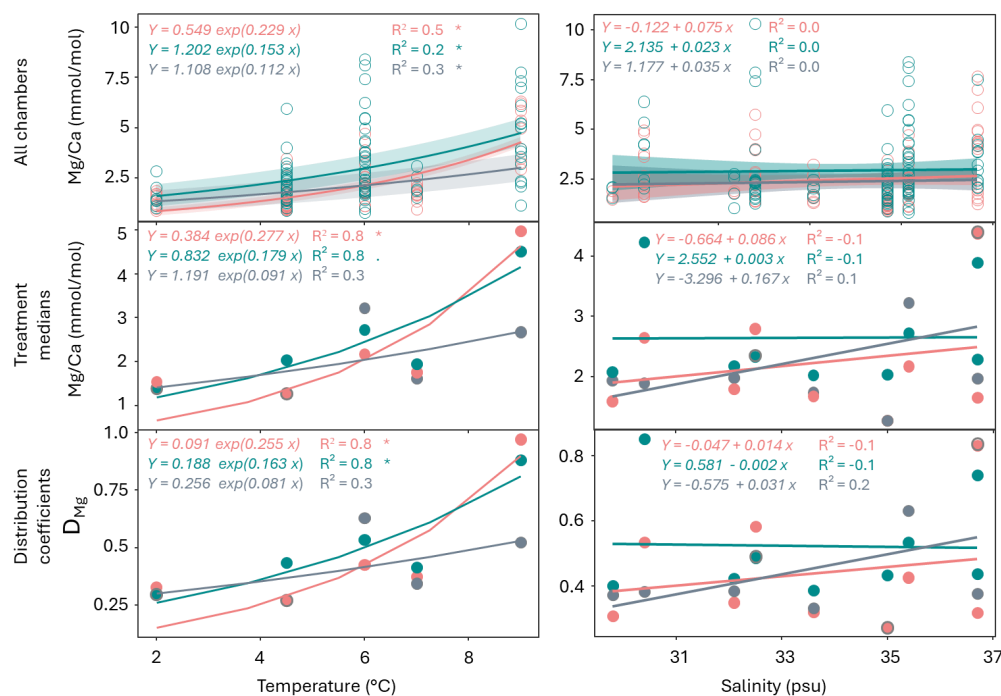
Water treatment	Mg/Ca (mmol/mol)			$D_{Mg/Ca} * 1000$			Shell wall (µm)	%crust (when both CC & LC present)	
	CC+LC	CC	LC	CC+LC	CC	LC			
Temperature (°C)	2	1.4 ±0.29	1.55 ±0.32	1.41 ±0.59	0.30	0.33	0.30	11	73
	4.5	1.28 ±0.64	1.28 ±0.59	2.04 ±1.09	0.27	0.27	0.43	17	62
	6	3.22 ±1.22	2.18 ±0.95	2.73 ±1.99	0.63	0.43	0.53	13	71
	7	1.62 ±0.14	1.77 ±0.36	1.95 ±0.56	0.34	0.37	0.41	12	60
	9	2.68 ±0.60	4.97 ±1.24	4.50 ±2.36	0.52	0.97	0.88	25	54
Salinity	29.8	1.94	1.60 ±0.17	2.09 ±0.51	0.37	0.31	0.4	24	87
	30.4	1.90 ±1.53	2.65 ±1.29	4.23 ±1.59	0.38	0.53	0.85	13	68
	32.1	1.99	1.81 ±0.06	2.19 ±0.69	0.38	0.35	0.42	14	76
	32.5	2.36 ±0.94	2.8 ±1.39	2.34 ±2.38	0.49	0.58	0.49	7	72
	33.6	1.74 ±0.51	1.68 ±0.63	2.03 ±0.31	0.33	0.32	0.39	15	68
	36.7-f	4.40 ±0.43	4.38 ±1.19	3.89 ±1.40	0.84	0.83	0.74	13	67
	36.7-e	1.98 ±0.14	1.67 ±0.29	2.30 ±0.17	0.38	0.32	0.44	14	57
pH and carbonate ion (pH total scale)	7.78	3.65 ±1.42	3.86 ±1.45	4.73 ±3.00	0.73	0.77	0.95	13	59
	7.83	2.93 ±1.32	2.48 ±1.32	3.27 ±1.91	0.57	0.48	0.64	12	58
	7.84	3.65	3.97 ±1.05	2.10 ±0.51	0.70	0.77	0.41	11	56
	8.26	1.54 ±0.64	1.55 ±0.81	1.79 ±0.70	0.30	0.30	0.34	14	62
	8.4	1.18	1.35 ±0.1	1.52 ±0.38	0.22	0.25	0.28	10	67
Carbonate ion (µmol/kg)	64	2.31	2.13 ±0.49	2.33 ±0.91	0.46	0.43	0.47	13	53
	195	4.73 ±1.37	3.19 ±1.56	3.44 ±1.55	0.92	0.62	0.67	11	66
	206	3.24 ±1.66	3.41 ±1.53	3.59 ±3.12	0.65	0.69	0.72	12	62
pH (decoupled carbonate ion)	7.65	6.59	4.26 ±1.73	8.65 ±2.64	1.33	0.86	1.75	8	63
	7.88	5.23 ±1.52	4.38 ±1.92	7.15 ±4.54	1.06	0.88	1.44	11	69
	8.15	2.15 ±0.34	1.91 ±0.58	2.23 ±0.36	0.44	0.39	0.45	23	37

304



305 **3.3 Temperature**

306 Mg/Ca has a significant positive exponential relationship ($p < 0.005$) with temperature in both the crust
 307 and lamellar calcite when all chambers are included (Fig. 2). Although R^2 may not be accurately
 308 representative for non-linear relationships, pseudo- R^2 was calculated to 0.5 and 0.2 in the crust and
 309 lamellar calcite respectively (Table 4). The pseudo- R^2 for both components combined is 0.3 with
 310 $p < 0.005$. The exponential curve is significantly steeper for the crust than lamellar calcite and the two
 311 curves therefore converge at higher temperatures ($> 9^\circ\text{C}$). The relationship is also significant in the crust
 312 treatment medians and both the crust and lamellae distribution coefficients.



313

314 *Figure 2. Element/Ca vs temperature (left) and salinity (right) regression lines with all chambers*
 315 *included (left), treatment medians (middle), and distribution coefficients (right). Pink line = crust, green*
 316 *line = lamellae, grey line = both combined. Statistical significance: * $p < 0.05$, . $p < 0.1$.*

317

318 **3.4 Salinity**



319 There is a weak positive relationship between Mg/Ca and salinity, however this is not significant ($p > 0.1$,
320 Fig. 2). Due to the methods used to modify the seawater salinity, DIC, $[\text{HCO}_3^-]$, and total alkalinity (TA)
321 co-varied linearly with salinity (Table 2), $[\text{CO}_3^{2-}]$ also varied between the salinity treatments, however
322 not linearly.

323

324 3.5 Carbonate chemistry

325 The three carbonate chemistry treatments (pH & $[\text{CO}_3^{2-}]$, pH, and $[\text{CO}_3^{2-}]$) all have significant influence
326 on Mg/Ca in the crust, lamellae and both components combined (Table 4, Fig. 3). There is a significant
327 negative correlation between Mg/Ca and pH (Fig. 3 left and middle panels). This relationship is steeper
328 (-4.7 compared to -7.3 mmol/mol decrease in Mg/Ca per pH unit based on crust in all chambers) when
329 $[\text{CO}_3^{2-}]$ does not co-vary with pH. The pH with co-varying $[\text{CO}_3^{2-}]$ (typical in nature) relationship with
330 Mg/Ca is significant for all chambers, treatment medians, and the distribution coefficients (Fig. 3 left
331 panel). When the two parameters do not co-vary, the relationship is not significant in the crust when
332 using treatment medians and distribution coefficients (Fig. 3 middle panel). There are significant
333 positive relationships between Mg/Ca and $[\text{CO}_3^{2-}]$ in the crust and lamellar calcite, but not the two
334 components combined (Fig. 3 right panel). When using treatment medians and distribution coefficients
335 the Mg/Ca- $[\text{CO}_3^{2-}]$ relationship is only significant in the lamellae. A plot of Mg/Ca correlated to pH
336 with co-varying $[\text{CO}_3^{2-}]$ with treatments performed at 6°C normalised to 4.5° using the temperature
337 relationships for crust, lamellar calcite, and both components separately (section 3.3) is shown in Fig.
338 S2 (Table S4).

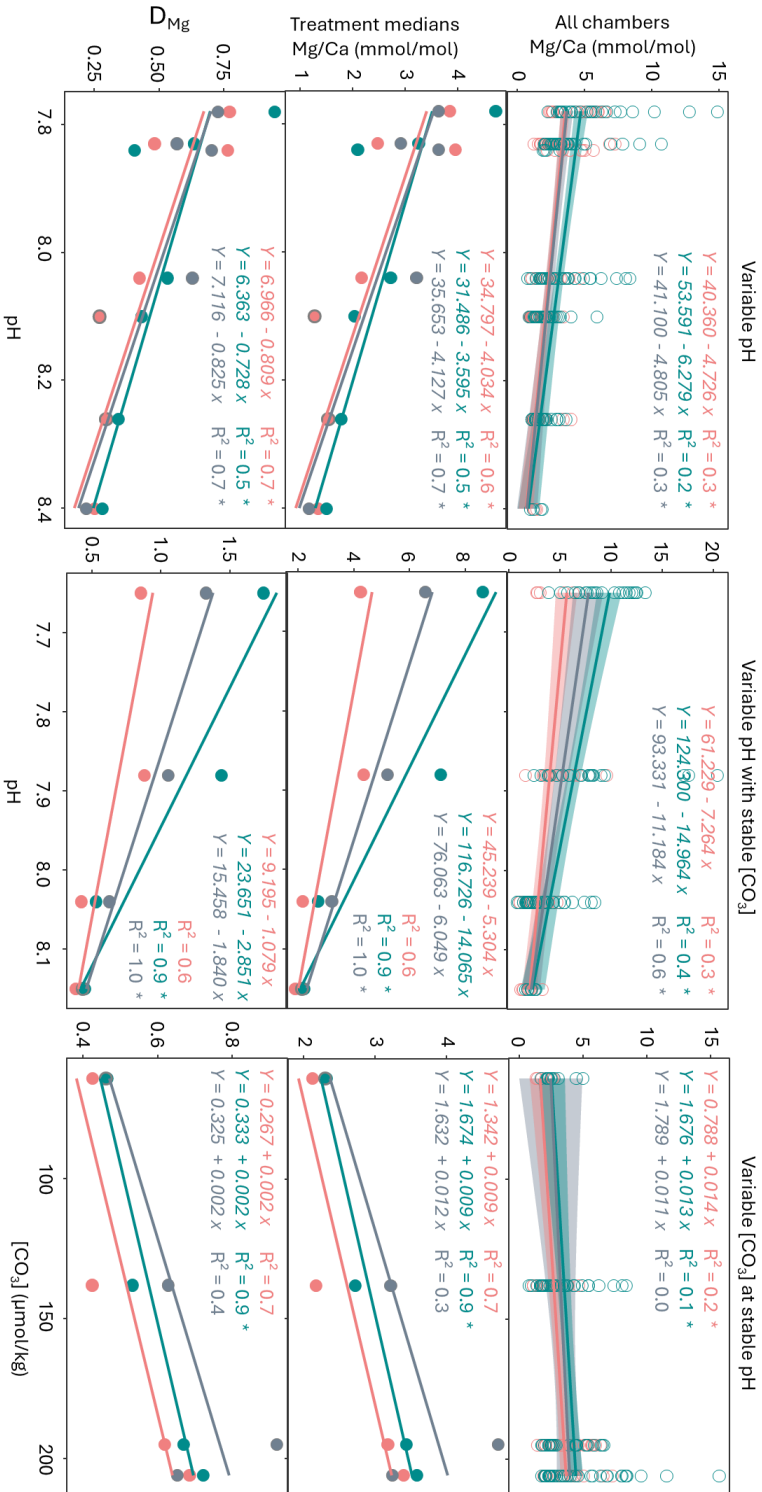


Figure 3. Regression lines for the Mg/Ca relationship with carbonate chemistry parameters. Mg/Ca (mmol/mol) for all chambers (top), Mg/Ca treatment medians (middle), and Partitioning coefficients (D_{Mg}; bottom). Pink line = crust, green line = lamellae, grey line = both combined. Statistical significance: *p < 0.05, **p < 0.01. See also Fig. S2.

339
 340
 341
 342
 343



344 **Table 4. Calibration equations, R^2 , and p -values for Mg/Ca relationship with temperature and carbonate chemistry in crust, lamellar calcite, and both**
 345 **components with all chambers included, treatment medians, and distribution coefficients (D_{Mg}). Only significant relationships are included.**

Mg/Ca relationship	Data type	Crust calcite:	Lamellar calcite:	Both components:
Mg/Ca temperature	All chambers	Mg/Ca = $0.549 \pm 0.099 \exp(0.229 \pm 0.024 T)$ $R^2 = 0.5$ $p = 4.45 * 10^{-14}$	Mg/Ca = $1.202 \pm 0.263 \exp(0.153 \pm 0.031 T)$ $R^2 = 0.2$ $p = 2.69 * 10^{-6}$	Mg/Ca = $1.108 \pm 0.249 \exp(0.112 \pm 0.035 T)$ $R^2 = 0.3$ $p = 0.003$
	Treatment medians	Mg/Ca = $0.384 \pm 0.259 \exp(0.277 \pm 0.084 T)$ $R^2 = 0.5$ $p = 0.05$		
	Distribution coefficients	Mg/Ca = $0.091 \pm 0.056 \exp(0.255 \pm 0.078 T)$ $R^2 = 0.8$ $p = 0.05$	Mg/Ca = $1.202 \pm 0.068 \exp(0.153 \pm 0.050 T)$ $R^2 = 0.8$ $p = 0.05$	
Mg/Ca pH with co-varying $[CO_3^{2-}]$	All chambers	Mg/Ca = $40.360 - 4.726 \text{ pH}$ $R^2 = 0.3$ $p = 7.6 * 10^{-12}$	Mg/Ca = $53.591 - 6.279 \text{ pH}$ $R^2 = 0.2$ $p = 1.4 * 10^{-10}$	Mg/Ca = $41.100 - 4.805 \text{ pH}$ $R^2 = 0.3$ $p = 2.5 * 10^{-7}$
	Treatment medians	Mg/Ca = $34.797 - 4.034 \text{ pH}$ $R^2 = 0.6$ $p = 0.02$	Mg/Ca = $31.486 - 3.595 \text{ pH}$ $R^2 = 0.5$ $p = 0.05$	Mg/Ca = $35.653 - 4.127 \text{ pH}$ $R^2 = 0.7$ $p = 0.01$
	Distribution coefficients	Mg/Ca = $6.966 - 0.809 \text{ pH}$ $R^2 = 0.7$ $p = 0.01$	Mg/Ca = $6.363 - 0.728 \text{ pH}$ $R^2 = 0.5$ $p = 0.05$	Mg/Ca = $7.116 - 0.825 \text{ pH}$ $R^2 = 0.7$ $p = 0.01$
Mg/Ca pH without co-varying $[CO_3^{2-}]$	All chambers	Mg/Ca = $61.229 - 7.264 \text{ pH}$ $R^2 = 0.3$ $p = 1.9 * 10^{-5}$	Mg/Ca = $124.300 - 14.964 \text{ pH}$ $R^2 = 0.4$ $p = 3.5 * 10^{-11}$	Mg/Ca = $93.331 - 11.184 \text{ pH}$ $R^2 = 0.6$ $p = 1.3 * 10^{-5}$
	Treatment medians		Mg/Ca = $116.726 - 14.065 \text{ pH}$ $R^2 = 0.9$ $p = 0.04$	Mg/Ca = $76.063 - 6.049 \text{ pH}$ $R^2 = 1.0$ $p = 0.01$
	Distribution coefficients		Mg/Ca = $23.651 - 2.851 \text{ pH}$ $R^2 = 0.9$ $p = 0.05$	Mg/Ca = $15.458 - 1.840 \text{ pH}$ $R^2 = 1.0$ $p = 0.01$
Mg/Ca $[CO_3^{2-}]$ without co-varying pH	All chambers	Mg/Ca = $0.788 + 0.014 [CO_3^{2-}]$ $R^2 = 0.2$ $p = 4.3 * 10^{-4}$	Mg/Ca = $1.676 + 0.013 [CO_3^{2-}]$ $R^2 = 0.1$ $p = 0.006$	
	Treatment medians		Mg/Ca = $1.342 + 0.009 [CO_3^{2-}]$ $R^2 = 0.9$ $p = 4.4 * 10^{-12}$	
	Distribution coefficients		Mg/Ca = $0.325 + 0.002 [CO_3^{2-}]$ $R^2 = 0.9$ $p = 0.04$	

346



347 4 Discussion

348 4.1 New Mg/Ca-temperature calibrations for the crust and lamellar calcite

349 The Mg/Ca-temperature relationship presented in this study substantially extends the culture-based
350 calibration range in this species from 9–12°C (c.f., Davis et al., 2017) to 2–7°C. While both the crust
351 and lamellar calcite have significant exponential Mg/Ca relationships with temperature, the Mg/Ca is
352 consistently lower in the crust than lamellar calcite at all temperatures. However, as shown in Westgård
353 et al. (2026), but confirmed here over a greater range of temperatures, the difference between the crust
354 and lamellae decreases with increasing temperature from ~23% higher Mg/Ca in the lamellae at 4.5°C
355 (largest difference) to 5% lower Mg/Ca in the lamellae at 9°C when comparing treatment medians. The
356 exponential curve for the crust is therefore steeper than for the lamellar calcite and thus, the calibration
357 curves converge at ~8°C using the treatment medians and or >9°C using all chambers (Fig. 2, 4). As the
358 habitat of *N. pachyderma* includes temperatures from <0 to >10°C, its use in palaeoreconstructions also
359 covers a wide range of temperatures. Therefore, temperatures obtained from the crust and lamellar
360 calcite will be appreciably different depending on the specimen's growth temperatures in most of this
361 temperature range.

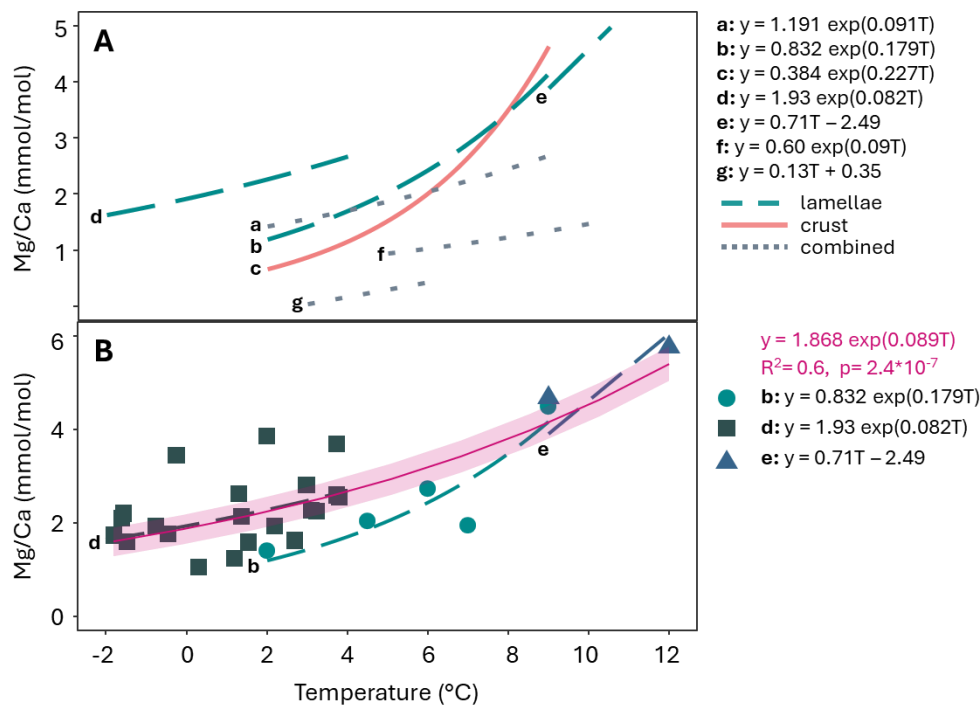
362 The steepness of the combined crust and lamellar calibration curve is strongly influenced by
363 crust:lamellae proportions as a larger proportion of crust will shift the specimen median value towards
364 the crust values or towards the lamellar median if the lamellar calcite is proportionally thicker. This also
365 introduces more variability and “noise” to the combined calibration curve. In addition, as we observe
366 proportionally less crust at higher temperatures (Fig. 1), calibrations based on both components are then
367 disproportionately influenced by lamellar values with increasing temperature with the overall effect of
368 decreasing temperature sensitivity (Fig. 4). As crust thickness varies with environmental conditions and
369 downcore in marine sediments, i.e., through time, this further complicates the application of whole-
370 specimen Mg/Ca-based temperature estimates from this species. We therefore reaffirm the need to
371 consider the two components separately in development and application of proxies in this species
372 (Jonkers et al., 2016; Davis et al., 2017; Livsey et al., 2020; Westgård et al., 2026). We thus recommend



373 using the calibration curves presented in this study for each component separately, which include the
374 first crust-only calibration.

375 The Mg/Ca values we obtain are largely comparable with previous culture and plankton-tow based
376 studies (i.e., Davis et al., 2017; Livsey et al., 2020) at equivalent temperatures (Fig. 4, panel B). The
377 lamellar calcite Mg/Ca-temperature calibration by Livsey et al. (2020) using *N. pachyderma* sampled
378 by plankton tow is similar to the lamellar curve obtained in this study, although their absolute values are
379 higher than our observations at the lower temperature range (<4°C). Thus by compiling the treatment
380 medians from this study, with the data from Davis et al. (2017) and the means from Livsey et al. (2020)
381 we present an extended calibration for the lamellar calcite (Fig 4, panel B). A comparable compilation
382 cannot be produced for the crust as such data is not published outside of this study.

383 The Mg/Ca values reported in this study, along with those from other studies analysed by LA-based
384 methods (e.g., Davis et al., 2017; Livsey et al., 2020) are higher than Mg/Ca values from sediment trap
385 and core top samples at equivalent temperatures analysed by solution-based approaches (Fig. 4, e.g.,
386 Jonkers et al., 2016; Kozdon et al., 2009a; Morley et al., 2024). This difference may partly reflect
387 variation in crust proportions, sample preservation, and potential loss of lamellar calcite during sample
388 handling for solution-based analyses (c.f., Westgård et al., 2026). Additional sources of uncertainty
389 include the estimation of true water temperatures for core-top samples, as growth temperatures can only
390 be approximated, and differences in single- versus multi-specimen cleaning procedures, which can affect
391 measured Mg/Ca values (Lee et al., 2025).



392

393 *Figure 4. Mg/Ca-temperature equations from this study plotted alongside published equations. A)*
 394 *Equations based on crust, lamellae, or both combined are indicated by colours pink, green, and grey*
 395 *respectively. a, b, c = This study, d = Livsey et al. (2020), e = Davis et al. (2017), f = Jonkers et al.*
 396 *(2013), and g = Kozdon et al. (2009a). Calibrations by Davis et al. (2017), and Livsey et al. (2020), are*
 397 *both based on lamellar calcite only and analysed by LA-ICP-MS. Calibrations by Jonkers et al. (2013)*
 398 *and Kozdon et al. (2009a), are based on wholeshell analysis by solution of crusted samples from*
 399 *sediment trap and core top respectively. B) Compilation of data and calibrations based on the lamellar*
 400 *calcite only with a combined lamellar calibration curve ($R^2 = 0.6, p = 2.4 \cdot 10^{-7}$).*

401

402 4.2 Carbonate chemistry and salinity influences on Mg/Ca

403 We observe significant carbonate chemistry influence on Mg/Ca, with opposite effects from pH
 404 (negative) and $[\text{CO}_3^{2-}]$ (positive) on both crust and lamellar calcite (Fig. 3, Table 4). When the two
 405 carbonate system parameters are decoupled, the negative Mg/Ca relationship with pH produces a steeper
 406 slope than the positive slope of $[\text{CO}_3^{2-}]$. This suggests pH exerts a stronger control on Mg/Ca than $[\text{CO}_3^{2-}]$.
 407]

408 This finding is in contrast to Davis et al. (2017) who observed no significant pH and/or $[\text{CO}_3^{2-}]$ (co-
 409 varied) influence on Mg/Ca in the closely related species, *Neogloboquadrina incompta*. Other studies



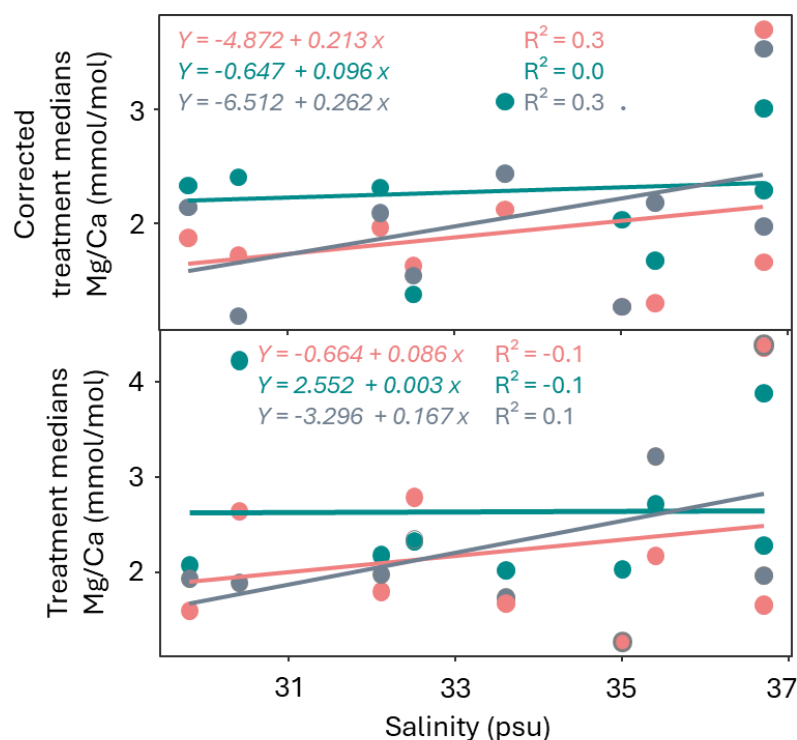
410 (Morley et al., 2024; Lea et al., 1999; Russell et al., 2004; Evans et al., 2018) have reported significant
411 carbonate chemistry influence on Mg/Ca however none of these decoupled pH from $[\text{CO}_3^{2-}]$ and/or
412 $[\text{HCO}_3^-]$ although Evans et al. (2018) decoupled pH and DIC. Some studies such as Morley et al. (2024)
413 on *N. pachyderma* and Russell et al. (2004); Allen et al. (2016) on multiple warm water species observed
414 a negative exponential relationship between Mg/Ca and seawater $[\text{CO}_3^{2-}]$. However, in these studies, pH
415 and $[\text{CO}_3^{2-}]$ likely co-vary (as is typical in nature) and thus the driving parameter could not be isolated.
416 Allen et al. (2016) also observed increased Mg/Ca with $[\text{CO}_3^{2-}]$ when pH was kept constant in *Trilobatus*
417 *sacculifer* ($R=0.96$, $p=0.04$) while it decreased when pH and $[\text{CO}_3^{2-}]$ co-varied, in line with our results
418 on *N. pachyderma*. We also obtain a significant negative Mg/Ca relationship with $[\text{CO}_3^{2-}]$ (and pH, Fig.
419 S3) in the pH treatment with co-varying $[\text{CO}_3^{2-}]$. This Mg/Ca- $[\text{CO}_3^{2-}]$ relationship is comparable that to
420 observed by Morley et al. (2024), with an overall decrease from ~ 5 to ~ 1 mmol/mol Mg/Ca over ~ 70 -
421 $240 \mu\text{mol/kg}$ $[\text{CO}_3^{2-}]$ (or pH 7.7-8.4 in our study, Fig. S3). However, we observe a negative relationship
422 between Mg/Ca and pH at “constant” $[\text{CO}_3^{2-}]$ (Fig. 3) and a positive relationship with $[\text{CO}_3^{2-}]$ at
423 “constant” pH (Fig. S3). Thus, the negative relationships and Russell et al. (2004); Allen et al. (2016);
424 Morley et al. (2024) observed likely also represent a negative relationship to pH (with co-varying $[\text{CO}_3^{2-}]$
425) rather than to $[\text{CO}_3^{2-}]$.

426 We observed a positive Mg/Ca sensitivity to salinity ($\sim 9\%$ and $\sim 0.3\%$ per salinity unit in crust and
427 lamellae respectively) comparable to other studies (3-5 %, e.g., Allen et al., 2016; Hönisch et al., 2013).
428 However, the Mg/Ca-salinity relationships in this study was not statistically significant , in line with
429 Bertlich et al. (2021). In our salinity experiments, carbonate chemistry and temperature were not always
430 fixed (Fig. S1, Table 2). Thus, for any temperature, pH, and $[\text{CO}_3^{2-}]$ values that are outside the standard
431 error of the T4.5°C treatment, we used our Mg/Ca-relationships from the temperature and carbonate
432 chemistry experiments (Table 4 & 5) to isolate the salinity effects on Mg/Ca. This results in a steeper
433 positive ($\sim 20\%$ and $\sim 10\%$ in crust and lamellae respectively) Mg/Ca-relationship with salinity (Fig. 5,
434 Table S4), however it is also not significant at the 95% confidence interval. As carbonate chemistry
435 often co-varies with salinity in nature (e.g., Olsen et al., 2020), the uncorrected salinity-Mg/Ca
436 relationship (in which carbonate chemistry and salinity covary) may represent the “natural”



437 salinity/carbonate chemistry effect in many settings and the pH, $[\text{CO}_3^{2-}]$, and salinity-influences on
438 Mg/Ca may therefore effectively cancel each other out. For example, meltwater intrusions leading to
439 concurrent freshening and pH decrease would have opposing impacts on foraminiferal Mg/Ca.

440 We observed significant differences in Mg/Ca between the two high (36.7) salinity treatments despite
441 all measured environmental parameters being equivalent (e.g., temperature, salinity, pH, and $[\text{CO}_3^{2-}]$,
442 Table 2). The two treatments were prepared differently by using rejection brine and evaporated seawater
443 (Section 2.2, and Table 2) and obtained statistically different Mg/Ca (e.g., crust values were 4.38 ± 1.19
444 and 1.67 ± 0.29 mmol/mol respectively). Although we cannot provide a mechanistic explanation, it is
445 worth noting that there were more laboratory-grown ($n=23$) and crusted chambers ($n=11$) in the
446 treatment prepared with rejected brine compared to the treatment made using evaporated seawater (only
447 6 lab-grown and crusted chambers in total, Table 3). This difference could be caused by random
448 variability or a “vital effect” caused by an unknown, not measured, variable which influences chamber
449 precipitation and Mg/Ca.



450



451 *Figure 5. The Mg/Ca relationship with salinity when corrected for influence by T, pH and [CO₃²⁻] (top)*
452 *and without correction (bottom, also in Fig. 2). Regression lines for Mg/Ca treatment medians*
453 *(mmol/mol). Pink line = crust, green line = lamellae, grey line = both combined. Statistical significance:*
454 **p<0.05, .p<0.1. Note the different y-axes.*

455

456 4.3 Crust-lamellae proportions are influenced by environmental conditions

457 Although crust formation occurred in all treatments, environmental conditions clearly influence the
458 proportion of crust to lamellar calcite. Increasing salinity is significantly correlated with lower crust
459 proportions (Fig. 1, Table 3 & S3). We also observed lower proportion of crust at lower pH, and higher
460 [CO₃²⁻] and temperatures, though not significantly at the 95% confidence level. Additionally, we observe
461 overall thinner shells at lower pH values. The general reduction of %crust and shell thickness with
462 decreasing pH and [CO₃²⁻] supports evidence of negative impacts of ocean acidification on shell
463 calcification (c.f., Chaabane et al., 2024; Manno et al., 2012; Anglada-Ortiz et al., 2021). Also, higher
464 temperatures, considered suboptimal for *N. pachyderma* in this region, were also associated with
465 reduced crust proportions, although thicker shells (c.f., Chaabane et al., 2024; Westgård et al., 2023).
466 These results thus indicate that crust and shell thickness is environmentally influenced and suggest
467 processes such as Atlantification (expansion of warm, saline Atlantic water to the Arctic, c.f., Ingvaldsen
468 et al., 2021) and ocean acidification may lead to reduced calcification in the future, with also potential
469 implications for carbon export and ballasting (c.f., Tell et al., 2022; Anglada-Ortiz et al., 2021).

470

471 4.4 Proxy calibration and implications for palaeoceanographic reconstructions

472 The presented Mg/Ca-calibration curves significantly extend the range covered by culture-based
473 calibrations in *N. pachyderma*, from 9–12°C (Davis et al., 2017) to 2–9°C. This has potential to
474 significantly improve temperature-reconstructions in the subpolar and polar regions where SSTs can be
475 as low as -2°C. In addition, we present a compilation calibration including data from Davis et al. (2017)



476 and Livsey et al. (2020), resulting in a combined calibration from -2 to 12°C for the lamellar calcite
477 (Fig. 4). However, crust often dominates the shell weight in the fossil record (40-80%, c.f., Westgård et
478 al., 2026; Kozdon et al., 2009a), and some studies report loss of the lamellar calcite during diagenesis,
479 handling, and/or cleaning, the crust calibration may therefore be more important in paleo-
480 reconstructions.

481 Both the difference in Mg/Ca between the crust and lamellae and the proportion of crust to lamellae vary
482 with environmental conditions, for example both decrease with temperature (Fig 1 & 2). In downcore
483 reconstructions, both aspects are sources of uncertainty. Increasing temperature leads to more influence
484 from the high-Mg/Ca lamellae, skewing temperature-estimates based on whole-shell analysis towards
485 higher temperatures. Therefore, not separating the two components results in inaccuracy and
486 uncertainties in temperature estimates. When both crust and lamellar calcite are present, they can be
487 separated by laser ablation analysis using the methods developed by Westgård et al. (2026) and the
488 corresponding Mg/Ca calibrations presented in this study can be applied to each component, thus
489 reducing the uncertainty introduced by crust-lamellar variations and differences.

490 Sea ice formation, meltwater input, and river discharge alter the carbonate chemistry and salinity of the
491 adjacent seawater (e.g., Fransson et al., 2013). We show that carbonate chemistry significantly
492 influences Mg/Ca in *N. pachyderma* (section 3.5 & 4.2) and should therefore be considered in
493 paleoclimate reconstructions in polar waters and sites influenced by these processes. However, the pH
494 influence on Mg/Ca appears to be less impactful in the pH range 8.1–8.4 (Fig. 3), which is the expected
495 range in the Quaternary pelagic Nordic Seas (e.g., Ezat et al., 2017), thus we expect limited pH influence
496 on Mg/Ca in this region on such timescales.

497

498 4.5 Implications for biomineralisation

499 The different responses of Mg/Ca in the crust and lamellar calcite to changing environmental parameters
500 suggests they calcify via different biomineralisation mechanisms, supporting previous findings
501 (Westgård et al., 2026). This particularly applies to the Mg/Ca-temperature and -pH relationships where



502 the difference between the two components decreases with increasing temperature and pH. Environment
503 also influences the total shell thickness and balance between these two components such that changes
504 in the environment therefore affects crust calcification in two ways: the final proportions of crust to
505 lamellae and the incorporation of trace elements into each component.

506 In this study Mg/Ca responds oppositely to changing pH and $[\text{CO}_3^{2-}]$, and we observe larger differences
507 in steepness of the slope of the relationship between the crust and lamellar calcite in response to pH but
508 not $[\text{CO}_3^{2-}]$ (Fig. 3). Increasing $[\text{CO}_3^{2-}]$ likely leads to increased calcite precipitation rates, which results
509 in higher D_{Mg} in inorganic precipitation experiments (e.g., Branson et al., 2025; Allen et al., 2016),
510 potentially explaining the positive Mg/Ca correlation with $[\text{CO}_3^{2-}]$. Such an increase can also be
511 explained by Rayleigh fractionation (c.f., Evans et al., 2018 and references therein) if the higher
512 calcification rates occurred from the same sized pool of Ca, where Mg abundance is $\sim 5x$ higher.

513 The Mg/Ca-relationship to pH with constant $[\text{CO}_3^{2-}]$ results in a steeper negative relationship (with
514 different slopes for the crust and lamellar calcite) compared to changing pH with co-varying $[\text{CO}_3^{2-}]$
515 (where the crust and lamellar calcite have relatively similar slopes), in-line with removal of a “[CO_3^{2-}]-
516 effect” on Mg/Ca. This suggests that there is a different driver behind the Mg/Ca response to pH than
517 the Mg/Ca response to $[\text{CO}_3^{2-}]$. We suggest that the Mg/Ca response to $[\text{CO}_3^{2-}]$ may be driven by
518 calcification rate (a physical process), but that the response to pH and the observed differences between
519 the crust and lamellar calcite may instead be driven by a physiological process. In particular,
520 foraminifera are thought to have a high pH-calcification fluid to aid calcification regulated by H^+ -
521 pumping (De Nooijer et al., 2009; Toyofuku et al., 2017). The low pH culture media would require the
522 specimen to increase the pH of its internal calcifying fluid more than at higher pH, at a higher energy-
523 cost (e.g., Morley et al., 2024; François et al., 2025; De Nooijer et al., 2009). This would leave less
524 energy available for Mg-removal from the site of calcification to counter the inhibiting effect Mg^{2+} has
525 on calcification (e.g., Zeebe and Sanyal, 2002; Jacob et al., 2017; De Nooijer et al., 2014; Westgård et
526 al., 2026), thus providing an explanation for the observed lower Mg/Ca ratios at lower pH (c.f., Evans
527 et al., 2018). This is also reflected in the thinner shells with a lower proportion of crust observed at lower
528 pH. Alternatively, the pH-effect on Mg/Ca could be explained if proton-removal via the enzyme Ca-



529 ATPase (e.g., Toyofuku et al., 2017) is less efficient at lower pH (e.g., Guo and Messer, 1978), thus also
530 transporting less Ca^{2+} at lower pH, resulting in higher Mg/Ca. Assuming *N. pachyderma* modulates the
531 pH of its calcifying fluid, high Mg/Ca at low pH does not align with recent findings for benthic
532 foraminifera (François et al., 2025) suggesting greater difference between seawater pH and the
533 calcification site is correlated with higher Ca^{2+} flux, as this would lead to lower Mg/Ca at lower pH
534 which is the opposite of what we observe (Fig. 3). This may imply that in planktic and benthic
535 foraminifera biomineralisation influences Mg/Ca in contrasting ways.

536 5 Conclusions

537 We present a range of laboratory-based investigations into the variability of Mg/Ca in
538 *Neogloboquadrina pachyderma* to a range of realistic past and future polar environmental parameters
539 including temperature, salinity, and carbonate chemistry with decoupled pH and $[\text{CO}_3^{2-}]$. We observe
540 that the proportion of crust in the shell in part is controlled by environmental conditions and decreases
541 significantly with increasing salinity, and not significantly with decreasing pH and $[\text{CO}_3^{2-}]$ and
542 increasing temperature. The total shell thickness also decreases with decreasing pH with implications
543 for downcore reconstructions, and foraminifera ecology and carbon export in relation to ongoing
544 climate change.

545 Using LA-ICP-MS and open-source code (Westgård et al., 2026) we were able to separate the
546 geochemical signals of crust and lamellar calcite, and observed significant differences in the two
547 components' Mg/Ca-sensitivity to environmental conditions (based on 525 lab-grown chambers, Table
548 S3). The new low-temperature Mg/Ca-temperature calibrations for *N. pachyderma* for the crust
549 ($\text{Mg/Ca} = 0.549 \pm 0.099 \exp^{(0.229 \pm 0.024T)}$) and lamellar calcite ($\text{Mg/Ca} = 1.202 \pm 0.263 \exp^{(0.153 \pm 0.031T)}$)
550 significantly extend the lower temperature range (from 9°C to 2°C) of culture-based Mg/Ca-
551 calibrations. By uncoupling the carbonate system parameters, we find that pH has significant negative
552 influence and $[\text{CO}_3^{2-}]$ has significant positive influence on Mg/Ca. When the two parameters co-vary,
553 pH is the primary driver of the relationship, causing a decrease in Mg/Ca with increasing pH & $[\text{CO}_3^{2-}]$



554] This impacts the interpretation of the Mg/Ca-proxy, particularly in regions subject to carbonate
555 chemistry changes, e.g., areas with sea-ice and meltwater input.

556 Separate proxy-calibrations for the crust and lamellar calcite therefore have the potential to significantly
557 reduce inaccuracies and uncertainty of polar palaeoreconstructions using *N. pachyderma* by accounting
558 for changes in crust-lamellar proportions downcore and their different sensitivity to environmental
559 conditions. Thanks to established analytical protocol by Westgård et al. (2026), the suggested separation
560 of shell component is time efficient and does not decrease data quality.

561 We suggest that the positive relationship we observe between Mg/Ca and $[\text{CO}_3^{2-}]$ reflects the influence
562 of increased precipitation rate at higher $[\text{CO}_3^{2-}]$ on D_{Mg} , as is observed in inorganic experiments (e.g.,
563 Branson et al., 2025 and references therein). Meanwhile the negative Mg/Ca-relationship with pH is
564 likely a physiological response, either driven by: i) less effective transport by Ca-ATPase at lower pH
565 or ii) due to the increased energetic cost of the enhanced levels of proton-pumping needed to elevate
566 calcifying fluid pH at lower seawater pH and the resulting reduction in energy available for Mg^{2+}
567 removal. This is supported by the observed thinner shells with lower crust% at lower pH.

568



569 Data availability

570 Associated data is uploaded to the open repository DataverseNO and a DOI will be provided upon article
571 acceptance.

572 Supplementary Material

573 Supplementary material includes figures S1, S2, and S3 showing correlations of culture media
574 parameters, temperature-normalised Mg/Ca (mmol/mol) correlated to pH with co-varying [CO₃],
575 and decoupling of the Mg/Ca-carbonate chemistry relationships. Table S1 gives an overview of
576 published results from each culture experiment. Table S2 shows Mg/Ca_{sw} in mmol/mol of culture
577 media. Table S3 shows the number of *N. pachyderma* chambers grown in culture per treatment, the
578 number of specimens with crust or lamellae only analysed, with both components analysed, and the
579 total number of chambers that grew crust in the lab. Table S4. Lists the corrected Mg/Ca (mmol/mol)
580 treatment medians corresponding to Fig. 5 and S2.

581 Author contributions

582 The study was designed by MME, AW, JM, GLF. AW, JM, MME, TC, and FS contributed to sample
583 collection and culturing. AW, GLF, and AM analysed the foraminifera samples, and MC analysed water
584 samples. MME contributed with finances and original research plan. AW wrote the first article draft,
585 and all authors contributed to the article and approved the version included in the thesis.

586 Competing interests

587 The authors declare no competing interests.

588 Acknowledgements

589 We thank the captains and crews of RV Helmer Hanssen and the UiT cruise- and laboratory-engineers;
590 Truls Holm, Karina Monsen, Ingvild Hald, Trine Dahl, Bjørn Runar Olsen and Matteus Lindgren for
591 their support with sampling and laboratory-work. We also thank Naima El bani Altuna, Christine
592 Lockwood-Ireland, Franziska Tell, Elwyn de la Vega, and Pushpak Martin for their support during



593 cruises and culturing. We thank Chris Standish, Matt Cooper and Alex Searle-Barnes at the University
594 of Southampton/NOC for analysing water samples and support with LA-ICP-MS analysis and Helene
595 Lødemel at the Institute of Marine Research for analysing carbonate chemistry water samples. We also
596 thank Nele Meckler and Jeroen Groeneveld for valuable discussions related to this study.

597

598 Funding

599 This study is funded through the ARCLIM project by the Tromsø Research Foundation (project number
600 A31720). This research is also part of the iC3: Centre for ice, Cryosphere, Carbon and Climate, project
601 number 332635 and the ERC synergy project i2B into the Blue, grant number 101118519. T.B.C was
602 supported by the ARCLIM project and ERC StG ForCry, grant number 101040461. GLF was supported
603 by NERC grant NE/W009552/1.

604



605 References

- 606 Allen, K. A., Hönisch, B., Eggins, S. M., Haynes, L. L., Rosenthal, Y., and Yu, J.: Trace element proxies for
607 surface ocean conditions: A synthesis of culture calibrations with planktic foraminifera, *Geochimica et*
608 *Cosmochimica Acta*, 193, 197–221, 10.1016/j.gca.2016.08.015, 2016.
- 609 AMAP: AMAP Assessment 2018: Arctic Ocean Acidification., 2018.
- 610 Anand, P., Elderfield, H., and Conte, M. H.: Calibration of Mg/Ca thermometry in planktonic
611 foraminifera from a sediment trap time series, *Paleoceanography*, 18, n/a–n/a,
612 10.1029/2002pa000846, 2003.
- 613 Anglada-Ortiz, G., Meilland, J., Ziveri, P., Chierici, M., Fransson, A., Jones, E., and Rasmussen, T. L.:
614 Seasonality of marine calcifiers in the northern Barents Sea: Spatiotemporal distribution of planktonic
615 foraminifers and shelled pteropods and their contribution to carbon dynamics, *Progress in*
616 *Oceanography*, 218, 103121, <https://doi.org/10.1016/j.pocean.2023.103121>, 2023.
- 617 Anglada-Ortiz, G., Zamelczyk, K., Meilland, J., Ziveri, P., Chierici, M., Fransson, A., and Rasmussen, T.
618 L.: Planktic Foraminiferal and Pteropod Contributions to Carbon Dynamics in the Arctic Ocean (North
619 Svalbard Margin), *Frontiers in Marine Science*, Volume 8 - 2021, 10.3389/fmars.2021.661158, 2021.
- 620 Barker, S., Greaves, M., and Elderfield, H.: A study of cleaning procedures used for foraminiferal
621 Mg/Ca paleothermometry, *Geochemistry, Geophysics, Geosystems*, 4,
622 <https://doi.org/10.1029/2003GC000559>, 2003.
- 623 Bertlich, J., Gussone, N., Berndt, J., Arlinghaus, H. F., and Dieckmann, G. S.: Salinity effects on cultured
624 *Neogloboquadrina pachyderma* (sinistral) from high latitudes: new paleoenvironmental insights, *Geo-*
625 *Marine Letters*, 41, 10.1007/s00367-020-00677-1, 2021.
- 626 Branson, O., Chauhan, N., Evans, D., Foster, G. L., and Rickaby, R. E. M.: Geochemical tracers of
627 biomineralisation processes, in: *Treatise on Geochemistry (Third edition)*, edited by: Anbar, A., and
628 Weis, D., Elsevier, Oxford, 177–235, <https://doi.org/10.1016/B978-0-323-99762-1.00128-5>, 2025.
- 629 Chaabane, S., Garidel-Thoron, T., Meilland, J., Sulpis, O., Chalk, T., Brummer, G.-J., Mortyn, P., Giraud,
630 X., Helene, H., Casajus, N., Kuroyanagi, A., Beaugrand, G., and Schiebel, R.: Migrating is not enough
631 for modern planktonic foraminifera in a changing ocean, *Nature*, 1–7, 10.1038/s41586-024-08191-5,
632 2024.
- 633 Davis, C. V., Fehrenbacher, J. S., Hill, T. M., Russell, A. D., and Spero, H. J.: Relationships Between
634 Temperature, pH, and Crusting on Mg/Ca Ratios in Laboratory-Grown *Neogloboquadrina*
635 Foraminifera, *Paleoceanography*, 32, 1137–1152, 10.1002/2017pa003111, 2017.
- 636 Davis, C. V., Livsey, C. M., Palmer, H., Hull, P., Thomas, E., Hill, T. M., and Benitez-Nelson, C.: Extensive
637 morphological variability in asexually produced planktic foraminifera, *Science Advances*, 6, 2020.
- 638 de Nooijer, L. J., Toyofuku, T., and Kitazato, H.: Foraminifera promote calcification by elevating their
639 intracellular pH, *Proceedings of the National Academy of Sciences*, 106, 15374–15378,
640 10.1073/pnas.0904306106, 2009.
- 641 de Nooijer, L. J., Spero, H. J., Erez, J., Bijma, J., and Reichert, G. J.: Biomineralization in perforate
642 foraminifera, *Earth-Science Reviews*, 135, 48–58, <https://doi.org/10.1016/j.earscirev.2014.03.013>,
643 2014.



- 644 Dickson, A. G., Sabine, C. L., and Christian, J. R., Dickson, A. G., Sabine, C. L., and Christian, J. R. (Eds.):
645 Guide to best practices for ocean CO₂ measurement, PICES Special Publication 3; IOCCP Report 8,
646 North Pacific Marine Science Organization, Sidney, British Columbia, 191 pp., 10.25607/obp-1342,
647 2007.
- 648 Elderfield, H. and Ganssen, G.: Past temperature and $\delta^{18}\text{O}$ of surface ocean waters inferred from
649 foraminiferal Mg/Ca ratios, *Nature*, 405, 442–445, 10.1038/35013033, 2000.
- 650 Evans, D., Müller, W., and Erez, J.: Assessing foraminifera biomineralisation models through trace
651 element data of cultures under variable seawater chemistry, *Geochimica et cosmochimica acta*, 236,
652 198–217, 10.1016/j.gca.2018.02.048, 2018.
- 653 Evans, D., Wade, B. S., Henehan, M., Erez, J., and Müller, W.: Revisiting carbonate chemistry controls
654 on planktic foraminifera Mg / Ca: implications for sea surface temperature and hydrology shifts over
655 the Paleocene–Eocene Thermal Maximum and Eocene–Oligocene transition, *Clim. Past*, 12, 819–835,
656 10.5194/cp-12-819-2016, 2016.
- 657 Eynaud, F., Cronin, T. M., Smith, S. A., Zaragosi, S., Mavel, J., Mary, Y., Mas, V., and Pujol, C.:
658 Morphological variability of the planktonic foraminifera *Neogloboquadrina pachyderma* from ACEX
659 cores: Implications for Late Pleistocene circulation in the Arctic Ocean, *Micropaleontology*, 55, 101–
660 116, 10.2307/40607109, 2009.
- 661 Ezat, M., Meilland, J., Westgård, A., Chalk, T., Sykes, F., El Bani Altuna, N., Nadar, P., Tell, F., and de la
662 Vega, E.: CAGE-ARCLIM cruise: Culturing (sub)Arctic planktic foraminifera *Neogloboquadrina*
663 *pachyderma* and *Globigerina bulloides*: Implications for ocean acidification and paleoceanography
664 reconstructions, CAGE – Centre for Arctic Gas Hydrate, Environment and Climate Report Series, 10,
665 10.7557/cage.6768, 2022.
- 666 Ezat, M. M., Fahl, K., and Rasmussen, T. L.: Arctic freshwater outflow suppressed Nordic Seas
667 overturning and oceanic heat transport during the Last Interglacial, *Nature Communications*, 15,
668 8998, 10.1038/s41467-024-53401-3, 2024.
- 669 Ezat, M. M., Rasmussen, T. L., Hönlisch, B., Groeneveld, J., and Demenocal, P.: Episodic release of CO₂
670 from the high-latitude North Atlantic Ocean during the last 135 kyr, *Nature Communications*, 8,
671 14498, 10.1038/ncomms14498, 2017.
- 672 Ezat, M. M., Meilland, J., Westgård, A., Chalk, T. B., Rasmussen, T. L., El Bani Altuna, N., and
673 Lockwood-Ireland, C.: Cruise Report: CAGE21-2- Planktic foraminifera sampling for culturing
674 experiments, central Greenland Sea 75°N, Department of Geosciences, UiT The Arctic University of
675 Norway, N-9037 Tromsø, 10.7557/cage.6714, 2021.
- 676 Fransson, A., Chierici, M., Miller, L. A., Carnat, G., Shadwick, E., Thomas, H., Pineault, S., and
677 Papakyriakou, T. N.: Impact of sea-ice processes on the carbonate system and ocean acidification at
678 the ice-water interface of the Amundsen Gulf, Arctic Ocean, *Journal of Geophysical Research: Oceans*,
679 118, 7001–7023, 10.1002/2013jc009164, 2013.
- 680 François, D., Reichert, G.-J., and de Nooijer, L. J.: Open or closed: pH modulation and calcification by
681 foraminifera, *Science Advances*, 11, eadq8425, doi:10.1126/sciadv.adq8425, 2025.
- 682 Fritz-Endres, T. and Fehrenbacher, J.: Preferential Loss of High Trace Element Bearing Inner Calcite in
683 Foraminifera During Physical and Chemical Cleaning, *Geochemistry, geophysics, geosystems* : G3, 22,
684 n/a, 10.1029/2020GC009419, 2021.



- 685 Greco, M., Jonkers, L., Kretschmer, K., Bijma, J., and Kucera, M.: Depth habitat of the planktonic
686 foraminifera *Neogloboquadrina pachyderma* in the northern high latitudes explained by sea-ice and
687 chlorophyll concentrations, *Biogeosciences*, 16, 3425–3437, 10.5194/bg-16-3425-2019, 2019.
- 688 Greco, M., Westgård, A., Sykes, F. E., Ezat, M. M., and Meilland, J.: Uncovering hidden structures:
689 previously undescribed pseudopodia and ectoplasmic structures in planktonic foraminifera, *Journal of*
690 *Plankton Research*, 10.1093/plankt/fbad031, 2023.
- 691 Guo, M. K. and Messer, H. H.: A comparison of Ca²⁺-, Mg²⁺-ATPase and alkaline phosphatase
692 activities of rat incisor pulp, *Calcified Tissue Research*, 26, 33–38, 10.1007/BF02013231, 1978.
- 693 Haynes, L. L., Hönisch, B., Holland, K., Eggins, S., and Rosenthal, Y.: Calibrating Non-Thermal Effects on
694 Planktic Foraminiferal Mg/Ca for Application Across the Cenozoic, *Paleoceanography and*
695 *Paleoclimatology*, 38, <https://doi.org/10.1029/2023PA004613>, 2023.
- 696 Holland, K., Branson, O., Haynes, L. L., Hönisch, B., Allen, K. A., Russell, A. D., Fehrenbacher, J. S.,
697 Spero, H. J., and Eggins, S. M.: Constraining multiple controls on planktic foraminifera Mg/Ca,
698 *Geochimica et Cosmochimica Acta*, 273, 116–136, 10.1016/j.gca.2020.01.015, 2020.
- 699 Hou, S., Toebrock, L., van der Linden, M., Rothstegge, F., Ziegler, M., Lourens, L. J., and Bijl, P. K.:
700 Southern Ocean control on atmospheric CO₂ changes across late Pliocene Marine Isotope Stage M2,
701 *Clim. Past*, 21, 79–93, 10.5194/cp-21-79-2025, 2025.
- 702 Hupp, B. N. and Fehrenbacher, J. S.: Geochemical differences between alive, uncrusted and dead,
703 crusted shells of *Neogloboquadrina pachyderma*: Implications for paleoreconstruction,
704 *Paleoceanography and Paleoclimatology*, 34, e2023PA004638,
705 <https://doi.org/10.1029/2023PA004638>, 2023.
- 706 Hupp, B. N. and Fehrenbacher, J. S.: Intratest trace element variability in polar and subpolar planktic
707 foraminifera: insights into vital effects, ontogeny, and biomineralization processes, *Journal of*
708 *Foraminiferal Research*, 54, 355–374, 10.61551/gsjfr.54.4.355, 2024.
- 709 Hönisch, B., Allen, K. A., Lea, D. W., Spero, H. J., Eggins, S. M., Arbuszewski, J., deMenocal, P.,
710 Rosenthal, Y., Russell, A. D., and Elderfield, H.: The influence of salinity on Mg/Ca in planktic
711 foraminifers – Evidence from cultures, core-top sediments and complementary δ¹⁸O, *Geochimica et*
712 *Cosmochimica Acta*, 121, 196–213, 10.1016/j.gca.2013.07.028, 2013.
- 713 Ingvaldsen, R. B., Assmann, K. M., Primicerio, R., Fossheim, M., Polyakov, I. V., and Dolgov, A. V.:
714 Physical manifestations and ecological implications of Arctic Atlantification, *Nature Reviews Earth &*
715 *Environment*, 10.1038/s43017-021-00228-x, 2021.
- 716 Inoue, M., Nohara, M., Okai, T., Suzuki, A., and Kawahata, H.: Concentrations of Trace Elements in
717 Carbonate Reference Materials Coral JCp-1 and Giant Clam Jct-1 by Inductively Coupled Plasma-Mass
718 Spectrometry, *Geostandards and Geoanalytical Research*, 28, 411–416,
719 <https://doi.org/10.1111/j.1751-908X.2004.tb00759.x>, 2004.
- 720 Jacob, D. E., Wirth, R., Agbaje, O. B. A., Branson, O., and Eggins, S. M.: Planktic foraminifera form their
721 shells via metastable carbonate phases, *Nature Communications*, 8, 10.1038/s41467-017-00955-0,
722 2017.
- 723 Jochum, K. P., Nohl, U., Herwig, K., Lammel, E., Stoll, B., and Hofmann, A. W.: GeoReM: A New
724 Geochemical Database for Reference Materials and Isotopic Standards, *Geostandards and*
725 *Geoanalytical Research*, 29, 333–338, <https://doi.org/10.1111/j.1751-908X.2005.tb00904.x>, 2005.



- 726 Jonkers, L., Buse, B., Brummer, G.-J. A., and Hall, I. R.: Chamber formation leads to Mg/Ca banding in
727 the planktonic foraminifer *Neogloboquadrina pachyderma*, *Earth and planetary science letters*, 451,
728 177–184, 10.1016/j.epsl.2016.07.030, 2016.
- 729 Jonkers, L., Jiménez-Amat, P., Mortyn, P. G., and Brummer, G.-J. A.: Seasonal Mg/Ca variability of *N.*
730 *pachyderma* (s) and *G. bulloides*: Implications for seawater temperature reconstruction, *Earth and*
731 *Planetary Science Letters*, 376, 137–144, <https://doi.org/10.1016/j.epsl.2013.06.019>, 2013.
- 732 Kohfeld, K. E., Fairbanks, R. G., Smith, S. L., and Walsh, I. D.: *Neogloboquadrina pachyderma* (sinistral
733 coiling) as paleoceanographic tracers in polar oceans: Evidence from northeast water polynya
734 plankton tows, sediment traps, and surface sediments, *Paleoceanography*, 11, 679–699,
735 10.1029/96pa02617, 1996.
- 736 Kozdon, R., Eisenhauer, A., Weinelt, M., Meland, M. Y., and Nürnberg, D.: Reassessing Mg/Ca
737 temperature calibrations of *Neogloboquadrina pachyderma* (sinistral) using paired $\delta^{44/40}\text{Ca}$ and
738 Mg/Ca measurements, *Geochemistry, Geophysics, Geosystems*, 10, n/a–n/a, 10.1029/2008gc002169,
739 2009a.
- 740 Kozdon, R., Ushikubo, T., Kita, N. T., Spicuzza, M., and Valley, J. W.: Intratest oxygen isotope variability
741 in the planktonic foraminifer *N. pachyderma*: Real vs. apparent vital effects by ion microprobe,
742 *Chemical Geology*, 258, 327–337, 10.1016/j.chemgeo.2008.10.032, 2009b.
- 743 Kucera, M.: Chapter Six Planktonic Foraminifera as Tracers of Past Oceanic Environments, in:
744 *Developments in Marine Geology*, edited by: Hillaire–Marcel, C., and De Vernal, A., Elsevier, 213–262,
745 [https://doi.org/10.1016/S1572-5480\(07\)01011-1](https://doi.org/10.1016/S1572-5480(07)01011-1), 2007.
- 746 Kucera, M., Weinelt, M., Kiefer, T., Pflaumann, U., Hayes, A., Weinelt, M., Chen, M.-T., Mix, A. C.,
747 Barrows, T. T., Cortijo, E., Duprat, J., Juggins, S., and Waelbroeck, C.: Reconstruction of sea-surface
748 temperatures from assemblages of planktonic foraminifera: multi-technique approach based on
749 geographically constrained calibration data sets and its application to glacial Atlantic and Pacific
750 Oceans, *Quaternary Science Reviews*, 24, 951–998, <https://doi.org/10.1016/j.quascirev.2004.07.014>,
751 2005.
- 752 Lea, D. W., Mashiotta, T. A., and Spero, H. J.: Controls on magnesium and strontium uptake in
753 planktonic foraminifera determined by live culturing, *Geochimica et Cosmochimica Acta*, 63, 2369–
754 2379, 0016-7037/99, 1999.
- 755 Lee, P.-T., Ho, S. L., Groeneveld, J., Mohtadi, M., Shen, C.-C., and Su, C.-C.: Effect of Cleaning
756 Procedures on the Mg/Ca Ratio of Single-Specimen Planktic Foraminifera, *Geochemistry, Geophysics,*
757 *Geosystems*, 26, e2024GC011975, <https://doi.org/10.1029/2024GC011975>, 2025.
- 758 Livsey, C. M., Kozdon, R., Bauch, D., Brummer, G. J. A., Jonkers, L., Orland, I., Hill, T. M., and Spero, H.
759 J.: High-Resolution Mg/Ca and $\delta^{18}\text{O}$ Patterns in Modern *Neogloboquadrina pachyderma* From the
760 Fram Strait and Irminger Sea, *Paleoceanography and Paleoclimatology*, 35,
761 <https://doi.org/10.1029/2020PA003969>, 2020.
- 762 Manno, C., Morata, N., and Bellerby, R.: Effect of ocean acidification and temperature increase on the
763 planktonic foraminifer *Neogloboquadrina pachyderma* (sinistral), *Polar Biology*, 35, 1311–1319,
764 10.1007/s00300-012-1174-7, 2012.
- 765 Meilland, J., Ezat, M. M., Westgård, A., Manno, C., Morard, R., Siccha, M., and Kucera, M.: Rare but
766 persistent asexual reproduction explains the success of planktonic foraminifera in polar oceans,
767 *Journal of Plankton Research*, 10.1093/plankt/fbac069, 2022.



- 768 Morley, A., de la Vega, E., Raitzsch, M., Bijma, J., Ninnemann, U., Foster, G. L., Chalk, T. B., Meilland, J.,
769 Cave, R. R., Büscher, J. V., and Kucera, M.: A solution for constraining past marine Polar Amplification,
770 Nature Communications, 15, 9002, 10.1038/s41467-024-53424-w, 2024.
- 771 Okai, T., Suzuki, A., Kawahata, H., Terashima, S., and Imai, N.: Preparation of a New Geological Survey
772 of Japan Geochemical Reference Material: Coral JCp-1, Geostandards Newsletter, 26, 95–99,
773 <https://doi.org/10.1111/j.1751-908X.2002.tb00627.x>, 2002.
- 774 Olsen, A., Lange, N., Key, R. M., Tanhua, T., Bittig, H. C., Kozyr, A., Álvarez, M., Azetsu-Scott, K., Becker,
775 S., Brown, P. J., Carter, B. R., Cotrim da Cunha, L., Feely, R. A., van Heuven, S., Hoppema, M., Ishii, M.,
776 Jeansson, E., Jutterström, S., Landa, C. S., Lauvset, S. K., Michaelis, P., Murata, A., Pérez, F. F., Pfeil, B.,
777 Schirnick, C., Steinfeldt, R., Suzuki, T., Tilbrook, B., Velo, A., Wanninkhof, R., and Woosley, R. J.: An
778 updated version of the global interior ocean biogeochemical data product, GLODAPv2.2020, Earth
779 Syst. Sci. Data, 12, 3653–3678, 10.5194/essd-12-3653-2020, 2020.
- 780 Paton, C., Hellstrom, J., Paul, B., Woodhead, J., and Hergt, J.: Iolite: Freeware for the visualisation and
781 processing of mass spectrometric data, Journal of Analytical Atomic Spectrometry, 26, 2508–2518,
782 10.1039/C1JA10172B, 2011.
- 783 Paul, B., Petrus, J., Savard, D., Woodhead, J., Hergt, J., Greig, A., Paton, C., and Rayner, P.: Time
784 resolved trace element calibration strategies for LA-ICP-MS, Journal of Analytical Atomic
785 Spectrometry, 38, 1995–2006, 10.1039/D3JA00037K, 2023.
- 786 Peral, M., Bassinot, F., Daëron, M., Blamart, D., Bonnin, J., Jorissen, F., Kissel, C., Michel, E.,
787 Waelbroeck, C., Rebaubier, H., and Gray, W. R.: On the combination of the planktonic foraminiferal
788 Mg/Ca, clumped ($\Delta 47$) and conventional ($\delta 18O$) stable isotope paleothermometers in
789 palaeoceanographic studies, Geochimica et cosmochimica acta, 339, 22–34,
790 10.1016/j.gca.2022.10.030, 2022.
- 791 Pierrot, D., Lewis, E., and Wallace, D.: CO2SYS DOS Program developed for CO2 system calculations,
792 ORNL/CDIAC-105. Carbon Dioxide Information Analysis Center, Oak Ridge National Laboratory, US
793 Department of Energy, Oak Ridge, TN, 2006.
- 794 Prabhakar, M., Thirumalai, K., Cronin, T. M., Gemery, L., Thomas, E. K., and Rafter, P. A.: Morphotypical
795 and Geochemical Variations of Planktic Foraminiferal Species in Siberian and Central Arctic Ocean
796 Core Tops, Journal of Foraminiferal Research, 54, 1–19, 10.61551/gsjfr.54.1.1, 2024.
- 797 RCoreTeam: R: A Language and Environment for Statistical Computing, R Foundation for Statistical
798 Computing [code], 2022.
- 799 Rodríguez-Sanz, L., Graham Mortyn, P., Martínez-García, A., Rosell-Melé, A., and Hall, I. R.: Glacial
800 Southern Ocean freshening at the onset of the Middle Pleistocene Climate Transition, Earth and
801 Planetary Science Letters, 345-348, 194–202, <https://doi.org/10.1016/j.epsl.2012.06.016>, 2012.
- 802 Russell, A. D., Hönisch, B., Spero, H. J., and Lea, D. W.: Effects of seawater carbonate ion concentration
803 and temperature on shell U, Mg, and Sr in cultured planktonic foraminifera, Geochimica et
804 Cosmochimica Acta, 68, 4347–4361, 10.1016/j.gca.2004.03.013, 2004.
- 805 Spindler, M. and Dieckmann, G. S.: Distribution and abundance of the planktic foraminifer
806 *Neogloboquadrina pachyderma* in sea ice of the Weddell Sea (Antarctica), Polar Biology, 5, 185–191,
807 10.1007/bf00441699, 1986.



- 808 Stein, R.: The Late Mesozoic-Cenozoic Arctic Ocean Climate and Sea Ice History: A Challenge for Past
809 and Future Scientific Ocean Drilling, *Paleoceanography and Paleoclimatology*, 34, 1851–1894,
810 <https://doi.org/10.1029/2018PA003433>, 2019.
- 811 Tell, F., Jonkers, L., Meilland, J., and Kucera, M.: Upper ocean flux of biogenic calcite produced by the
812 Arctic planktonic foraminifera *Neogloboquadrina pachyderma*, 10.5194/bg-2022-59, 2022.
- 813 Tierney, J. E., Malevich, S. B., Gray, W., Vetter, L., and Thirumalai, K.: Bayesian Calibration of the
814 Mg/Ca Paleothermometer in Planktic Foraminifera, *Paleoceanography and Paleoclimatology*, 34,
815 2005–2030, 10.1029/2019PA003744, 2019.
- 816 Toyofuku, T., Matsuo, M. Y., De Nooijer, L. J., Nagai, Y., Kawada, S., Fujita, K., Reichart, G.-J., Nomaki,
817 H., Tsuchiya, M., Sakaguchi, H., and Kitazato, H.: Proton pumping accompanies calcification in
818 foraminifera, *Nature Communications*, 8, 14145, 10.1038/ncomms14145, 2017.
- 819 Vázquez Riveiros, N., Govin, A., Waelbroeck, C., Mackensen, A., Michel, E., Moreira, S., Bouinot, T.,
820 Caillon, N., Orgun, A., and Brandon, M.: Mg/Ca thermometry in planktic foraminifera: Improving
821 paleotemperature estimations for *G. bulloides* and *N. pachyderma* left, *Geochemistry, Geophysics,*
822 *Geosystems*, 17, 1249–1264, <https://doi.org/10.1002/2015GC006234>, 2016.
- 823 Westgård, A., Ezat, M. M., Chalk, T. B., Chierici, M., Foster, G. L., and Meilland, J.: Large-scale culturing
824 of *Neogloboquadrina pachyderma*, its growth in, and tolerance of, variable environmental conditions,
825 *Journal of Plankton Research*, 10.1093/plankt/fbad034, 2023.
- 826 Westgård, A., Ezat, M. M., Sykes, F. E., Foster, G. L., Meilland, J., Chalk, T. B., and Milton, J. A.:
827 Laboratory-grown crust in planktic foraminifera *Neogloboquadrina pachyderma*; insights into
828 resolving inaccuracies in polar palaeotemperature estimates, *Geochimica et Cosmochimica Acta*,
829 <https://doi.org/10.1016/j.gca.2026.04.027>, 2026.
- 830 Zeebe, R. E. and Sanyal, A.: Comparison of two potential strategies of planktonic foraminifera for
831 house building: Mg²⁺ or H⁺ removal?, *Geochimica et Cosmochimica Acta*, 66, 1159–1169,
832 [https://doi.org/10.1016/S0016-7037\(01\)00852-3](https://doi.org/10.1016/S0016-7037(01)00852-3), 2002.
- 833